Quantitative biochemical profiling of GCase activity and α-synuclein proteoforms in postmortem human brains from GBA-related and idiopathic Parkinson's disease

Martino Luca Morella
m.morella@amsterdamumc.nl
Amsterdam UMC, Vrije Universiteit Amsterdam
Martha Teneketzi
Amsterdam UMC, Vrije Universiteit Amsterdam
Federico Ferraro
University Medical Center Rotterdam
Tim E Moors
Amsterdam UMC, Vrije Universiteit Amsterdam
Walter A Boiten
Amsterdam UMC, Vrije Universiteit Amsterdam
John JP Breve
Amsterdam UMC, Vrije Universiteit Amsterdam
Angela MT Ingrassia
Amsterdam UMC, Vrije Universiteit Amsterdam
Hanneke Geut
Amsterdam UMC, Vrije Universiteit Amsterdam
Lasse Pihlstrøm
Oslo University Hospital
Vinod Udayar
Roche Innovation Center, F. Hoffmann-La Roche
Vincenzo Bonifati
University Medical Center Rotterdam
Wilma DJ Berg
Amsterdam UMC, Vrije Universiteit Amsterdam

Article

Keywords: alpha-synuclein, truncated alpha-synuclein, glucocerebrosidase, GBA1 variants - lysosomal dysfunction, biochemistry, AlphaLISA.

Posted Date: April 10th, 2026

DOI: https://doi.org/10.21203/rs.3.rs-9264325/v1

Additional Declarations: No competing interests reported.

Abstract

Parkinson's disease (PD) is characterized by α-synuclein (αSyn) deposition and lysosomal dysfunction. Variants in the *GBA1* gene, which encodes for lysosomal glucocerebrosidase (GCase), are PD risk factors (GBA-PD) and have been associated with increased cortical involvement compared to idiopathic PD (IPD). Nonetheless, the relationship between αSyn accumulation and GCase deficiency remains unclear. This study aims to quantitatively define the biochemical relationship between GCase deficiency and αSyn proteoforms across brain regions in GBA-related and IPD. Here, we sequenced *GBA1* in 160 postmortem brains (25 iLBD, 114 PD, 21 controls) and conducted a comprehensive region-resolved quantitative biochemical analysis of the Locus coeruleus (LC), substantia nigra (SN) and medial temporal gyrus (GTM). The tissue was sequentially extracted to yield Soluble and Insoluble fractions for the measurement of Total, Ser129-phosphorylated (pSer129), and C-terminally truncated at aa122 (CTT122) αSyn proteoforms, and for the quantification of GCase activity and GCase protein levels. *GBA1* variants were detected in 21.9% of PD cases, including a novel frameshift variant. Disease-associated αSyn accumulation was observed only in the Insoluble pool. Insoluble pSer129 and CTT122 αSyn were markedly increased in both iLBD and PD, whereas Soluble species were unchanged. Insoluble pSer129 αSyn was undetectable in controls. Cortical, as well as midbrain αSyn burden did not differ between GBA-PD and IPD. Interestingly, GCase activity was substantially reduced in GBA-PD and in IPD across regions. pSer129 αSyn burden inversely correlated with GCase activity, both in the presence (GBA-PD) and absence (IPD) of *GBA1* variants. Overall, we demonstrate that aggregated, pSer129-enriched αSyn and GCase deficiency are biochemically linked across the PD spectrum independently of *GBA1* status and support therapies enhancing lysosomal/GCase function in both genetic and idiopathic PD.

Introduction

Parkinson's disease (PD) is a common age-related neurodegenerative disorder typically accompanied by the formation of Lewy bodies (LBs) and Lewy neurites throughout the brain [1]. These inclusion bodies are primarily composed of aggregated α-synuclein (αSyn) protein [2, 3]. The accumulation of αSyn into insoluble deposits (collectively termed Lewy pathology) is a common molecular feature of PD [4–6]. This aberrant protein aggregation is thought to result from impaired protein clearance mechanisms and is central to PD pathogenesis at the cellular level. LBs are often associated with other cellular components (e.g. lipids, mitochondria and organellar material) and reflect a failure of neuronal processes in association with the presence of misfolded proteins [7, 8]. The molecular events related to αSyn deposition are incompletely understood and could drive disease progression.

αSyn is a 140-amino-acid protein abundantly expressed in the brain, especially at presynaptic terminals [9, 10]. In its native state, αSyn is unfolded and highly dynamic, and it is thought to play a role in synaptic vesicle trafficking and neurotransmitter release [11, 12]. However, in PD and related disorders, αSyn undergoes misfolding and aggregation into oligomers and fibrils [13–15]. A variety of post-translational modifications (PTMs) on αSyn have been identified in LBs and in brain lysates [16, 17]. αSyn can be phosphorylated, ubiquitinated, nitrated, and C-terminally truncated (CTT), among other modifications. Many of these PTMs are enriched in pathological αSyn aggregates: they may influence clearance, promote aggregation, or occur as a consequence of aggregation. Understanding αSyn's PTMs is critical, as they may offer clues to disease mechanisms and potential therapeutic targets for intervening in αSyn pathology.

Among the various PTMs of αSyn, phosphorylation at serine-129 (pSer129) has gained particular attention in PD. This specific modification is common in the pathological αSyn found in PD brains and is widely used as a marker of αSyn pathology. Antibodies against pSer129 αSyn are commonly employed to label and quantify LB load in postmortem brain tissue [7, 18]. However, the functional significance of Ser129 phosphorylation of αSyn is still under investigation [19–22]. Similarly, CTT αSyn at Asparagine-122 (CTT122) has also been associated with the presence of PD and is enriched in the diseased brain [7, 23].

A critical molecular player in PD is the *GBA1* gene, which encodes the enzyme β-glucocerebrosidase (GCase). GCase is a lysosomal hydrolase responsible for the lysis of Glucosylceramide (GlcCer), among other substrates [24–26]. In the rare inherited disorder Gaucher's disease, loss-of-function variants in both copies of *GBA1* lead to greatly reduced GCase activity, causing the accumulation of GlcCer and other glycosphingolipids in cells and resulting in severe systemic and neurological symptoms [27, 28]. However, heterozygous *GBA1* risk variants, or mild homozygous risk variants, do not cause Gaucher's disease but have been identified as one of the most common coding genetic risk factors for PD [29, 30]. Individuals carrying a single *GBA1* risk variant have a significantly elevated likelihood of developing PD in their lifetime, with odds ratios reported between about 0.3–30.4, depending on variant severity [29, 31, 32]. *GBA1* variants are found in 3.2–31.3% of PD patients, depending on the population [29]. Patents with GBA-related PD (GBA-PD) have been reported to have earlier age at onset (of 1.7-6.0 years) and more severe clinical progression compared to idiopathic PD (IPD), including increased occurrence of cognitive dysfunction, dementia, and more frequent hallucinations [30, 33, 34]. Some studies have shown increased LB load in the cerebral cortex in GBA-PD compared to IPD, depending on the area [35–39]. *GBA1* risk variants have been demonstrated to be more frequent in cases with a clinical profile matching dementia with LB (DLB) compared to PD, suggesting an increased cortical involvement in *GBA1* variant carriers [40, 41]. Nonetheless, other studies reported no difference in cortical LB load in GBA-PD compared to IPD cases in both Soluble and Insoluble fractions [42, 43].

The unique association between *GBA1* mild risk variants and PD suggests that even partial GCase deficiency can contribute to PD pathogenesis and widespread αSyn pathology. Partial reduction in GCase activity in IPD has been previously reported, depending on study and anatomical area [38, 39, 44–47]. Experimental studies have shown that when GCase activity is reduced (whether by *GBA1* variants, pharmacological inhibition, or aging-related decline), cells accumulate more αSyn [48–52]. Conversely, there is evidence that the relationship is bi-directional: the presence of aggregated or excess αSyn itself can interfere with normal lysosomal function and may specifically impair GCase activity [48]. This might create a detrimental feedback loop where reduced GCase activity leads to αSyn accumulation, and accumulating αSyn further inhibits GCase. It is yet unclear whether GCase deficiency contributes to a significant increase in αSyn levels in the brain in GBA-PD, as well as in and IPD. This understanding is highly relevant for therapeutic strategies aiming to increase GCase activity in PD [53, 54].

In this study, we aimed to quantitatively define the biochemical relationship between GCase deficiency and αSyn proteoforms in human postmortem brain tissue of GBA-PD and IPD patients. Here, we studied absolute αSyn proteoform concentrations (Total, pSer129, CTT122) and GCase (total activity, protein

abundance, specific activity) using quantitative high-throughput biochemical readouts. We analysed different biochemical fractions of post mortem brain tissue from a *GBA1*-genotyped cohort spanning controls, iLBD and IPD with sampling from 3 brain regions (locus coeruleus (LC), substantia nigra (SN), medial temporal gyrus (GTM), to obtain severity-graded *GBA1* subgroups, and a region-resolved depiction of the αSyn-GCase axis. We found *GBA1* risk variants in 21.9% of PD cases, including one novel *GBA1* variant, and a marked accumulation of pSer129 and CTT122 αSyn in iLBD and PD, only in the Insoluble fraction. Insoluble αSyn concentration did not differ between IPD and GBA-PD or between *GBA1* variants severity. Importantly, GCase activity was reduced in both the GBA-PD and IPD group compared to controls across regions, and it strongly correlated with pSer129 αSyn levels both in the presence (GBA-PD) and absence (IPD) of *GBA1* risk variants. Overall, our comprehensive biochemical analyses of neuropathologically-characterized postmortem human brain samples argues against increased cortical αSyn load in GBA-PD compared to IPD and identifies a link between GCase activity and αSyn levels independently of *GBA1* status, supporting the potential use of GCase-targeting therapeutic approaches in both GBA-related and idiopathic PD.

Materials and methods

Postmortem human frozen tissue cohorts

Postmortem human brain tissue was obtained from either the Netherlands Brain Bank (NBB; www.brainbank.nl) or Normal Aging Brain Collection Amsterdam biobank (NABCA; www.nabca.eu) from neuropathologically verified donors. Informed consent for brain autopsy, use of brain tissue, and sharing of clinical information for research was obtained from either the donors or their families, adhering to all local ethical and legal guidelines. Brain dissections followed standard operating protocols established by the NBB, with neuropathological assessments conducted by a qualified neuropathologist [55, 56].

For the *GBA1 genotyping cohort*, we identified cases with a neuropathologically confirmed clinical diagnosis of PD, with or without dementia (PDD), who exhibited Lewy body disease (LBD) pathology and of which frozen brainstem and GTM tissue was available in the brain banks archives. We excluded cases with severe Alzheimer's disease pathology (Braak NFT stage > 3 and Thal phase > 3; n = 114) [1, 57]. Cases with severe cerebral amyloid angiopathy (CAA) type 1 pathology or microinfarcts were also excluded. Control cases had no detectable αSyn pathology (Braak αSyn stage 0) and were required to have "none" or "low" AD pathology (n = 21). Control cases with Braak αSyn stage > 0 were included as incidental LBD (iLBD) cases (n = 25). The demographic information of this cohort (*genotyping cohort*) and details on the *GBA1* risk variants identified are presented in Table 1 and Table 2. Fresh-frozen cerebellum blocks from the selected cases were obtained for DNA extraction and *GBA1* genotyping.

Based on tissue availability, 86 cases from the *genotyping cohort* were selected for biochemical analyses (10 controls, 14 iLBD, 40 IPD, 22 GBA-PD). To improve statistical power and ensure that sufficient tissue was available from every brain region, we established a *biochemistry cohort* by including additional cases from our brain bank for which genotyping information of *GBA1* was already available from earlier studies [44, 58]. The same inclusion criteria used for the *genotyping cohort* were applied to these additional cases. 52 cases met these criteria: 16 controls, 16 iLBD and 20 PD cases. 4 PD brains (3 IPD and 1 GBA-PD) originated from [44] and had been Sanger-sequenced for *GBA*, whereas the remaining 48 cases (16 controls, 16 iLBD, 7 IPD and 9 GBA-PD) came from [58], where *GBA1* status had been determined with the Infinium NeuroChip Consortium array [59] and supplemented with the imputation of additional variants. These additional cases included one control and one iLBD brain carrying the E326K variant (see Suppl. Table 2), which were not included in the presented biochemistry analysis, except for the analysis presented in Fig. 7–8. The resulting cohort (*biochemistry cohort*) consisted of 26 control cases (CTRL), 30 iLBD cases and 50 PD cases without a *GBA1* missense variant (CTRL), and 32 PD cases with a *GBA1* missense variants (GBA-PD). For details on the demographics of the *biochemistry cohort*, see Table 1, Supplementary Table 2, and Supplementary File 1. Additional clinical information, such as presence of dementia, age at death, age at disease onset (age at onset), disease duration, time interval from motor symptoms to dementia development, and presence of visual hallucinations were retrieved from clinical files and are reported in Supplementary File 2.

DNA purification

To isolate purified DNA for the sequencing of *GBA1* from fresh-frozen cerebellum blocks, about 30 mG of tissue were obtained from the blocks by cryosectioning using a cryostat (CryoStar NX50, Epredia). The DNA was purified using NucleoSpin DNA Lipid Tissue kit (#740471.50; Macherey-Nagel) following the protocol of the producer. Briefly, tissue was disrupted in MN Bead Tubes (Type D) using the kit lysis buffer (Buffer LT) with Proteinase K, and the clarified lysate was applied to silica-membrane spin columns. Columns were washed according to the manufacturer's protocol and genomic DNA was eluted in Elution Buffer BE. To minimize RNA carryover prior to quantification, an RNase A treatment step was included according to protocol. Initial quality and concentration of the obtained genomic DNA (gDNA) was assessed by measuring absorbance (A) at 230 nm (A230), 260 nm (A260) and 280 nm (A280) wavelength with a Nanodrop spectrophotometer (NanoDrop Lite Plus, Thermo Fisher Scientific Inc.). An A260/A280 ratio of > 1.7, an A260/A230 ratio of > 1.8 and a concentration of at least (5 nG/μL) were used as cutoff to proceed with sample analysis.

GBA1 genotyping

-*GBA1* sequencing

GBA1 gene in the *genotyping cohort* was performed at GenomeScan B.V. (Leiden, The Netherlands) in accordance to a previously established protocol [60]. Quality check of the gDNA samples was performed using a fragment analyser (Fragment Analyzer System, Agilent Technologies Inc.). Precise DNA concentration was determined using a Quant-IT measurement (Quant-iT dsDNA Assay Kit, Thermo Fisher Scientific Inc). A long-range PCR using TaKaRa LA Taq DNA Polymerase Hot-Start (#RR042B, Takara Bio USA Inc.) and target-specific primers were used to amplify *GBA1* [60]. After library preparation (NEBNext Ultra II Ligation Module, #E7595, New England Biolabs), amplicons were fragmented with Bioruptor Pico (Diagenode Inc.). A-tailing and ligation of sequencing adapters of the resulting product was performed according to the NEBNext Ultra II Ligation Module Instruction Manual (New England Biolabs).

Quality check was performed with a fragment analyser (Fragment Analyzer System, Agilent Technologies Inc.). Finally, sequencing was performed on an Illumina Novaseq 6000 System (Illumina Inc.).

-Sequencing data analysis

Quality of raw data was inspected using FastQC v.0.11.9 [61]. Next, sequencing adapters were removed using Trimmomatic v.0.39 [62], allowing a maximum of 2 mismatches and a minimum alignment score 12. Sickle v.1.33 [63] was used to trim and filter the paired reads. Bases were required to have a minimum PHRED score of Q30, and the splitted reads to have a minimum length of 36bp. QC-passing reads were mapped against *GBAP1*-masked GRChg37/hg19 reference genome using the Burrows-Wheeler algorithm (BWA-mem v. 0.7.17b [64]). After duplicates marking, the GATK v.4.2.4.1 [65] guidelines were followed to identify the variants. Coverage was calculated over the genomic interval chr1:155204151–155211199 using GATK DeptOfCoverage. Samples with a median read depth below 30x were excluded from downstream analyses, with 4 samples being filtered out. The number of variants in the region chr1:155204151–155211199 per sample were inspected to identify outliers. No sample had a number of variants bigger than the mean plus 3 standard deviations. Variants were deemed of interest if: 1 – In any of the samples passing both the "Sample read depth" and "Number of variants called" quality criteria as described above; 2 – Falling in the transcript NM_000157.3; 3 – Exonic or within ± 5 bp from canonical splice site. Variants were further annotated in silico using CADD [66] and GERP [67] scores from WGSA v0.85 [68] and the allele frequency from public databases including gnomAD [69] and GoNL [70]. Splicing effect was predicted using ADA, RF [71], SpliceAI [72] from WGSA v0.85 and SQUIRLS v.1.0.0 [73]. The identified variants are presented in Table 2 and Supplementary Table 1. *GBA1* variant severity was determined according to their association with Gaucher disease (GD) type II or III (severe), type I (intermediate) or with Parkinson's disease (mild), corresponding to Parlar et al. using the *GBA1-PD browser*, when available [31]. Frameshift and null variants were considered as severe (see Table 2 and Suppl. Table 1).

Imputation of GBA1 variants from microarray genotyping

For the samples genotyped on the Infinium NeuroChip Consortium Array (Illumina, San Diego, CA USA), initial quality checks and filtering were performed as described in a previous publication [74]. Imputation was performed using the Michigan Imputation Server [75] with European ancestry reference data from the Haplotype Reference Consortium [76].

Tissue sectioning

Fresh-frozen tissue blocks were manually dissected to isolate the areas of interest of the LC, SN and GTM blocks (Suppl. Figure 1). After incision, the tissue was cut in 60 µM sections using a cryostat (CryoStar NX50, Epredia). Several tubes of about 10 mG of tissue (wet weight) were produced for the different analysis by collecting sections from the area of interest per each block and kept frozen. The tissue was anonymized during cutting. Blocks of the brainstem at the level of the pons and containing the locus coeruleus (LC) were incised to separate the pons from the tegmentum, containing the LC (referred as LC; Suppl. Figure 1a). Blocks of the midbrain were incised to isolate the SN area (referred as SN; Suppl. Figure 1b). Blocks of the GTM were incised to isolate grey matter and discard the white matter (referred as GTM; Suppl. Figure 1c). The tissue collected during cryo-sectioning and used for further biochemical analysis.

Tissue fractionation

Tissue processing was randomized and anonymized to exclude technical biases and performed separately per brain region. For the quantification of total GCase enzyme activity and GCase protein levels by ELISA, the tissue was extracted in GCase Lysis Solution (McIlvaine buffer (100mM di-Sodium Hydrogen Phosphate Dihydrate, 50mM Citric Acid Monohydrate, pH 5.2) containing 0.25% (v/v) Triton X-100 (#108603, Millipore), cOmplete Protease Inhibitor Cocktail (#04693116001, Roche; according to manufacturer instruction) and PhosSTOP (#4906837001, Roche; according to manufacturer instruction)). 250 µL of GCase lysis solution at room temperature (RT) was added to each tube of 10 mG of frozen tissue sections, which was then inverted 10 times and vortexed (5 seconds, maximum speed). The sample was subsequently homogenized using a tissue dissociator (TissueLyser LT, Qiagen) with a single 5 mm stainless steel bead (#69989, Qiagen) per tube (50 Hz for 2 minutes at RT). The tube was then incubated in ice for 30 minutes and the homogenate was then centrifuged at 15,000 × G for 15 minutes at 4°C to separate the pellet and supernatant. The supernatant was divided into single-use aliquots and stored at -80°C until further analysis.

For the quantification of αSyn protein levels by AlphaLISA, the tissue was subjected to sequential protein extraction (Suppl. Figure 2) with a procedure adapted from published protocols [23, 77, 78]. First, 10 mG of tissue was thawed on ice and immediately incubated in 250 µL of SDS-free RIPA (RIPA Buffer (10X), #9806, Cell Signaling Technologies) containing 2% octyl-b-D-glucoside (w/v; #850511, Avanti Polar Lipids LLC.), 1 mM phenylmethylsulfonyl fluoride (PMSF), cOmplete Protease Inhibitor Cocktail (according to manufacturer instruction) and PhosSTOP (according to manufacturer instruction) (OG-RIPA). The tissue was then homogenized using a tissue dissociator (TissueLyser LT, Qiagen) with a single stainless-steel bead per tube (50 Hz for 2 min at RT) and then incubated in ice for 20 minutes. 200 µL of the homogenate was then transferred in an ultracentrifuge tube (0.2 mL Open-Top Thickwall Polycarbonate Tube, #343775, Beckman Coulter Inc.) and centrifuged at 100'000g at 4°C for 1 hour in an ultracentrifuge (Optima MAX-TL, Beckman Coulter Inc.). After ultracentrifugation, the supernatant was collected and stored at – 80°C in single-use aliquots. This fraction contains OG-RIPA-soluble, non-aggregated and membrane associated proteins ("Soluble" fraction). Subsequently, the resulting pellet (Pellet 1) was resuspended in 200 µL and centrifuged again at 100'000g at 4°C for 30 minutes to remove all remaining OG-RIPA-soluble protein. The resulting pellet was then solubilized in volume of UTC buffer (7M Urea, 2M Thiourea, 4% CHAPS, 30mM Tris/HCl) equal to 100 µL per mG of total protein in the Soluble fraction measured by BCA assay (#A55864, Thermo Fisher Scientific Inc.). The solution was then sonicated with a probe sonicator (Ultrasonics Sonifier 250, Branson) for 100 seconds (3 seconds on, 7 seconds off) and incubated at 100°C for 10 minutes. The sample was then centrifuged at 100'000g at 4°C for 30 minutes to yield an insoluble pellet (Pellet 2) and a

supernatant containing OG-RIPA-insoluble and UTC-soluble proteins (“Insoluble” fraction). The Insoluble fraction was stored in single-use aliquots at − 80°C for further analysis.

GCase enzymatic activity quantification

The total GCase enzyme activity assay was based on the conversion of the artificial GCase substrate Resorufin-β-D-glucopyranoside and was adapted from previously-published protocols for the high-throughput use in 384-wells plates in postmortem human brain lysate [44, 79–81]. One single-use aliquots from samples extracted with GCase Lysis Solution were initially thawed on ice and their protein concentration was measured by BCA in a 384-well format. In order to run all the samples at the same time and in the same plate, a second aliquot per each sample was thawed in ice an transferred to a 384-wells pre-dilution plate (Polypropylene Storage microplates, # 3657, Corning Inc.) by diluting it to 0.5 mG/mL in GCase Lysis Buffer. From the pre-dilution plate, an aliquot was taken to run a second BCA assay in a 384-well format for normalization on total protein. From the same pre-dilution plate, 5 µL of each sample and a blank (GCase Lysis Buffer) were transferred in triplicate to a black 384-well plate (#732–3724, VWR International LLC) for GCase enzyme activity measurement. Similarly, 5 µL of a dilution series of recombinant human GCase enzyme (Recombinant Human Glucosylceramidase, #7410-GHB-020, Bio-Techne) was prepared in GCase Lysis Solution (concentration in plate 0-2000 nG/mL) and added to the plate. 25 µL of GCase Assay Buffer (McIlvaine Buffer (Citrate/Phosphate buffer, 0.15M, pH 5.2) with 0.25% (w/v) of Taurocholic acid (#T4009, Sigma-Aldrich)) and 30 µL of Res-β-Glc-Substrate solution (Resorufin-β-D-glucopyranoside, #R4758, Sigma-Aldrich; 40µM Resorufin-β-glucopyranoside in GCase Assay Buffer) per each well (final substrate concentration 20 µM). All wells were then brought to 60 µL with GCase Assay Buffer. In parallel, a standard curve with free Resorufin (#73144, Sigma-Aldrich) was prepared in GCase Assay Buffer and diluted 1:2 with GCase Assay Buffer to a final volume of 60 µL per each well (final concentration: 0–20 µM) and added to the plate. Both the plate and all solutions were pre-warmed at 37°C. The plate was then sealed with a transparent plastic sealer (TopSeal-A PLUS, #6050185, Revvity), spun down (2000g x 10 seconds) a shaken for 1 min in an orbital vibrating shaker. The plate was then incubated at 37°C in a spectrophotometer (SpectraMax iD3, Molecular Devices LLC.) and the fluorescence of free resorufin was read (excitation: 535 nm, emission: 595nm) every 1 hour for 12 hours.

The enzymatic activity was calculated using R (R version 4.3.2, 2023-10-31) [82] by fitting a 4-parameter logistic curve to the free Resorufin standard curve to compute the moles or free resorufin product formed at each time point. The rate of reaction was then calculated per each time point (nmol/hour), normalized on total protein concentration (previously measured by BCA assay) and reported as median nmol of Resorufin product per hour per mG of total protein (nmol/hour/mG). Representative standard curves for the assay are presented in Supplementary Fig. 3 (Liner range 30–2000 nG/mL of hrGCase; Lower limit of detection (LLOD) = 49.5 nG/mL hrGCase; Lower limit of quantification (LLOQ) = 150.0 nG/mL hrGCase).

GCase protein levels quantification by ELISA

The ELISA assay to measure GCase protein levels in postmortem human brain lysate was developed using recombinant rabbit monoclonal anti-GCase antibody EPR26755-29 (Abcam ab309228; Capture antibody) and recombinant rabbit monoclonal anti-GCase antibody EPR26755-42 (Abcam ab309229; Detection antibody). The Detection antibody was biotinylated with a biotinylation kit (Biotin Conjugation Kit (Fast, Type A), #ab201795, Abcam) following manufacturer instructions. The first day, 30 µL of a 2 µG/µL Capture antibody solution in Coating Buffer (0.1 M Sodium Carbonate/Bicarbonate, pH 9.4) was added to each well of a high binding 384-well black plate (Immuno Plates, #460518, Thermo Fisher Scientific Inc.) and incubated overnight at 4°C. On the second day, each well was washed four times with 60 µL of Base Buffer (TBS (0.15 M NaCl, 0.050 M Tris-HCl, pH 7.2) + 0.05% Tween-20) and incubated for 1,5 hours at RT with 90 µL of Blocking Buffer (2% w/v BSA (Bovine Serum Albumin Fraction V, #03117332001, Roche) + 5% v/v Normal Rabbit Serum (#011-000-120, Jackson ImmunoResearch LTD.). Then, one single-use aliquot from the samples extracted with GCase Lysis Solution were initially thawed on ice and their protein concentration was measured by BCA in a 384-well format. In order to run all the samples at the same time and in the same plate, a second aliquot per each sample was thawed in ice and transferred to a 384-wells pre-dilution plate (Polypropylene Storage microplates, # 3657, Corning Inc.) and diluted to 1 mG/mL in GCase Lysis Buffer. From the pre-dilution plate, an aliquot was taken to run a BCA assay in a 384-well format for normalization on total protein. A second aliquot was taken from the pre-dilution plate to produce a second pre-dilution plate where the samples were diluted 1:10 in Sample Diluent (2% w/v BSA in Base Buffer). A standard curve with a serial dilution (0–10’000 pG/mL) of recombinant human GCase (Recombinant Human Glucosylceramidase, #7410-GHB-020, Bio-Techne) was prepared in Sample Diluent containing the same amount of GCase Lysis buffer as the samples (1:10) and added to the plate. Then, the Blocking Buffer was removed from the ELISA plate and 30 µL of diluted samples and standards were added and incubated for 2 hours at RT shaking (500 RPM). After, the wells were washed three times for 2 minutes with 60 µL of Washing Buffer and incubated with 30 µL of biotinylated Detection antibody solution (2 µG/mL in Sample Diluent) for 1 hour at RT shaking (500 RPM). The wells were then washed 6 times with 60 µL of Washing Buffer for 3 minutes and incubated with 30 µL of Sreptavidin HRP solution (50 nG/ml Streptavidin-HRP (#N100, Thermo Fisher Inc.) in Sample diluent) for 1 hour at RT. After, the wells were washed 6 times with 60 µL of Washing Buffer for 3 minutes and 30 µL of LumiPhos solution (LumiPhos-HRP, #PSA-100, Lumigen; according to manufacturer indication) was added to each well. After 5 minutes at RT, luminescence was read at a spectrophotometer (SpectraMax iD3, Molecular Devices LLC.). A representative standard curve for the assay is presented in Supplementary Fig. 4. The assay was linear between 30 and 4000 pG/mL. GCase protein concentration in the samples was calculated based on the standard curve by interpolating a 5-parameter logistic curve using the software GraphPad Prism (10.2.0, GraphPad Software) and by normalizing the values on the total protein concentration as measured by BCA.

α-synuclein proteoforms quantification by AlphaLISA

Quantification of αSyn proteoforms was performed with an AlphaLISA assay (Revvity), adapting the protocol from Moors et al. [23] and following the manufacturer’s recommendations to target three αSyn species: phosphorylated Ser129 (pSer129), truncated at αSyn122 (CTT122), and a C-terminal region encompassing residues 118–123 (referred as “Total” αSyn). A biotinylated antibody directed against the NAC domain of αSyn (Biotin anti-α-Synuclein, Clone A15115A, #848306, BioLegend; epitope aa80–96) served as the universal detection antibody. Specific acceptor antibodies — Syn-142 (gift Roche, [23]) for

pSer129, MJFR1 (#ab209420, Abcam) for the "Total", and A15127A (#848402, BioLegend) for CTT122 — were conjugated to AlphaLISA Acceptor Beads (Unconjugated AlphaLISA Acceptor Beads, #6772002, Revvity) at a 10:1 beads-to-antibody weight ratio. No cross-reactivity was observed between the assays. For the Total αSyn assay, MJFR1 conjugate detected 76% of pSer129 αSyn and did not recognize CTT122 αSyn (see Suppl. Figure 5g). Each pair of antibodies underwent concentration optimization to achieve robust signal-to-noise ratios without reaching the hook point.

To run all the samples at the same time and in the same plate, sample aliquots were thawed in ice and total protein amounts were measured by either BCA assay (Soluble samples) or Pierce 660nm assay (Insoluble samples). A master plate (Polypropylene Storage microplates, # 3657, Corning Inc.) was then prepared from a second sample aliquot as to equalize the concentration of all samples to either 3 mG/mL (Soluble samples) or 1.2 mG/mL (Insoluble samples) by diluting them in Assay Buffer (25 mM HEPES (#H3375, Sigma-Aldrich), 0.5% (v/v) Triton X-100 (#8603, Merck Millipore), 0.1% (w/v) Casein (# C0376, Sigma-Aldrich), and 0.1% (w/v) Dextran (Dextran-500, #9219.3, Carl Roth)). From the master plate, an aliquot was taken to run a second BCA assay (Soluble samples) or Pierce 660nm Assay (Insoluble samples) in a 384-well format for the normalization of the results on total protein. For the Soluble fractions, aliquots from the master plate were further diluted in Assay Buffer to 1:100 and 1:600 in pre-dilution plates. These diluted samples were used to run the pSer129, CTT122 (Dilution 1:100) and the Total (dilution 1:600) αSyn AlphaLISA assays. For the Insoluble fractions, aliquots from the master plate were further diluted in Assay Buffer to 1:90 and 1:270 in pre-dilution plates. These diluted samples were used to run the pSer129, CTT122 (Dilution 1:90) and Total (dilution 1:270) αSyn AlphaLISA assays.

Assays were conducted in 384-well AlphaPlates (#6005350, Revvity) with a 50 µL total volume per well. Standard curves were generated using recombinant wild-type αSyn (#S-1001-2, rPeptide), pSer129 (#RP-004, Proteos), and CTT122 (gift Roche, [23]) in the same buffer conditions (same OG-RIPA or UTC buffer dilution) as for the lysate samples (see Suppl. Figure 5). For each well, 5 µL of either diluted sample or recombinant standard was combined with 10 µL of Acceptor Beads conjugated to the respective Acceptor Antibody (75 µG/mL in the Total and CTT122 αSyn assays, 50 µG/mL in the pSer129 assay). The plate was then shaken for 1 minute and incubated at room temperature (RT) in the dark for 2 hours. Next, 10 µL of the biotinylated detection antibody (5 nM in Assay Buffer) was added, followed by another 1-minute shake and a 1-hour incubation under the same conditions. Then, 25 µL of Streptavidin Donor Beads (AlphaScreen Streptavidin Donor Beads, Revvity, Cat. 6760002) at 80 µG/mL was added per well. After shaking for 1 minute, the plate was incubated for an additional 30 minutes at RT in the dark. All samples were then measured on a VICTOR Nivo reader (PerkinElmer). All samples were run in triplicate. Data was graphed and analysed using R (R version 4.3.2, 2023-10-31) by fitting a 4-parameter logistic model to the standard curves to quantify αSyn levels in the samples (see Suppl. Figure 5). The lower limit of detection (LLOD) and lower limit of quantification (LLOQ) were computed calculated as the concentration at $\beta * 3.3\sigma$ (for LLOD) and $\beta * 10\sigma$ (for LLOQ) where σ is the standard deviation of the blank signal and β is the signal of the blank. Sample signal lower than the signal of the LLOD were considered as negative (undetectable) and reported as 0 pG/mL. A list of the antibodies used, their concentration and LLOD and LLOQ values per each assay are presented in Supplementary Table 2. All cases were measured in triplicate and mean values calculated per each case. The assays had a 6.6–10.0% coefficient of variance (CoV) in the Soluble assays (Total: 6.6%; pSer129: 8.2%; CTT122: 10.0%) and of 5.3-7.0% CoV in the Insoluble assays (Total: 7.0%; pSer129: 5.3%; CTT122: 5.6%) across all measurements.

Statistics and computing

The data were analysed and graphed using R (R version 4.3.2, 2023-10-31) and R Studio [83]. Graphs were created using the *ggplot2* R package [84] and graphical methods were created with BioRender (BioRender.com, 2025). Figures were composed using Inkscape (Inkscape 1.3, Inkscape.org). All statistical comparisons were adjusted using age, sex, and postmortem delay (PMD) as covariates (See Suppl. Figure 6). Outliers were handled by capping values above 1.5× the interquartile range (IQR) beyond the third quartile (Q3) within each group, and zero values (if present) were offset by a small constant (+ 0.03). In all tests, significance threshold was set at $p \leq 0.05$. When comparing multiple groups for a given outcome, a generalized linear model (GLM) with a Gamma distribution and identity link was fitted. As data from the CTT122 AlphaLISA assay followed a non-normal Tweedie distribution, here we used a GLM model with Tweedie family to examine group differences. When comparing the disease groups irrespective of the anatomical area, a gamma generalized linear mixed-effects model with log link was used with disease group as the primary fixed effect, anatomical region, age at death, sex and PMD as covariates, and a random intercept for each case. For subpopulations described by a covariate, the corresponding covariate was removed from the model. When significant, pairwise group comparisons were performed using the package *emmeans* (version 1.10.6) to generate estimated marginal means with a Tukey's p value adjustment for multiple comparisons. Values and percentage difference for each comparison reported in the text are based on median values. When comparing two groups for a continuous variable, a one-way ANCOVA was performed using group as the main factor and including covariates (age, sex, PMD) in the model. When comparing two groups for binary outcomes, we used a GLM with a binomial distribution and logit link was fitted, with group and relevant covariates (age, sex, PMD) included as predictors. Receiver operating characteristic (ROC) analysis was performed using logistic regression, and the area under the curve (AUC) with 95% confidence intervals was calculated. The optimal threshold for each variable was determined using Youden's J statistic [85], defined as *sensitivity + specificity − 1*. Correlation analysis was performed using a Pearson's correlation test (continuous variables) or a Spearman's correlation test (ordinal variables). Correlation coefficients and the associated p-values are reported in the figures. Multiple correlation was performed by computing pairwise Pearson's correlations among all the variables of interest. The statistical test used in each comparison is indicated in the figure legend.

Results

Study design and cohort description

In this study, we first performed full *GBA1* sequencing on postmortem human brains (n = 160) from iLBD (n = 25), PD (n = 114), and control cases (n = 21) to identify PD donors carrying (GBA-PD) or lacking (IPD) *GBA1* risk variants (*genotyping cohort*; Fig. 1; Table 1). Based on tissue availability, 86 cases out of the 160 cases from the *genotyping cohort* were selected for quantitative biochemical analyses (10 controls, 14 iLBD, 40 IPD, 22 GBA-PD). To increase statistical power and ensure balanced regional sampling, we then incorporated 52 additional brains (16 controls, 16 iLBD, and 20 PD) from previous GBA-genotyped cohorts [44, 58], yielding a final *biochemistry cohort* of 138 individuals (26 controls, 30 iLBD, 50 IPD, 32 GBA-PD; Table 1), which was used for the biochemical

analysis (Fig. 1). In the *biochemistry cohort*, IPD and GBA-PD groups contained proportionally fewer females than the control and iLBD groups (all $p < 0.05$; Female: control = 68%, iLBD = 62%, IPD = 36%, GBA-PD = 31%; Suppl. Figure 6a). Median age at death was significantly higher in the iLBD group than in any other group (all $p < 0.005$; +7.7–10.5%; Suppl. Figure 6b), whereas postmortem delay (PMD) was shorter in both IPD and GBA-PD groups than in controls (-17.8 and − 20.5% respectively; all $p < 0.05$; Suppl. Figure 6c). Because sex, age at death and PMD differed between groups, all subsequent statistical models were adjusted for these variables. Full demographic, clinical and neuropathological information of the *biochemistry cohort* is summarized in Table 1.

Table 1

Demographics, clinical and pathological characteristics of the GBA1 genotyping cohort and biochemistry cohort. Braak α-synuclein (αSyn) stage according to [86]. Braak stage for Neurofibrillary Tangles according to Montine, T.J., *et al.* [87]. CERAD Amyloid Plaque score according to Mirra, S.S., *et al.* [88]. Thal phase according to Thal, D.R., *et al.* [57]. LC = locus coeruleus; SN = substantia nigra; GTM = gyrus temporalis medius.

		Controls (N = 21)	iLBD (N = 25)	PD (N = 114)		
				All	IPD	GBA-PD
Genotyping cohort		*Nr = 21*	*Nr = 25*	*Nr = 114*	*Nr = 89*	*Nr = 25*
Age of death (Mean yrs ± SD)		76 ± 7.5	86 ± 7.3	77 ± 8.6	78 ± 8.7	75 ± 8.0
Sex (M/F)		13/8	11/14	70/44	59/30	15/15
Postmortem delay (Mean hrs ± SD)		8.3 ± 4.3	6.5 ± 1.5	10.6 ± 1.7	10.6 ± 1.5	6.11 ± 2.1
Braak αSyn stage (nr.)		0 (21)	1–5 (4/4/6/4/4); Atypical (3)	3–6 (1/5/35/73)	3–6 (1/5/29/54)	5–6 (6/24)
Braak stage for Neurofibrillary Tangles (nr.)		0–4 (2/10/5/3/1)	0–4 (2/9/4/8/2)	0–4 (9/42/35/22/4); n.a. (2)	0–4 (7/31/24/21/4) n.a. (2)	0–3 (2/11/11/1)
Thal phase (nr.)		0–3 (9/7/3/3)	0–3 (5/10/2/1); n.a. (7)	0–4 (29/36/10/30/8); n.a. (1)	0–4 (20/30/9/22/7); n.a. (1)	0–4 (9/6/1/8/1)
Biochemistry cohort		*Nr = 26*	*Nr = 30*	*Nr = 82*	*Nr = 50*	*Nr = 32*
Age of death (Mean yrs ± SD)		77 ± 8.9	84 ± 8.5	77 ± 8.3	78 ± 8.3	76 ± 8.6
Sex (M/F)		8/18	12/18	54/28	32/18	22/10
Postmortem delay (Mean min ± SD)		7.3 ± 1.2	6.8 ± 1.7	5.4 ± 1.5	5.8 ± 1.5	6.0 ± 1.5
Braak αSyn stage (nr.)		0 (26)	1–5 (5/3/13/6/2); Atypical (1)	5–6 (29/53)	5–6 (20/30)	5–6 (9/23)
Braak stage for Neurofibrillary Tangles (nr.)		0–3 (4/11/8/3)	0–4 (3/6/9/11)	0–4 (9/33/26/13/1)	0–4 (7/18/15/9/1)	0–3 (2/15/11/4)
Thal phase (nr.)		0–3 (7/5/6/7); n.a. (1)	0–3 (2/9/6/2); n.a. (11)	0–4 (23/20/10/22/6); n.a. (1)	0–4 (13/13/7/11/5); n.a. (1)	0–4(10/7/3/11/1)
Tissue blocks (nr.)	**LC**	17	19	35	20	15
	SN	13	14	26	20	6
	GTM	19	24	72	43	29

Table 2
Detailed information of the risk variants identified in the *GBA1 genotyping co*

Cohort					
Position on Chr 1 (hg19/GRCh37)	**Ref**	**Alt**	**NM_000157.3**	**pNomen**	**Allelic Name**
Missense					
155205540	GGGACTGTCGACAAAGTTACGCACCCAATTGGGTCCTCCTTCGGGGTTCAGGGCAA	G	c.1265_1319del	p.(Leu422fs)	L383fs (RecΔ55 /
155205634	T	C	c.1226A > G	p.(Asn409Ser)	N370S /
155206037	G	A	c.1223C > T	p.(Thr408Met)	T369M /
155206158	G	A	c.1102C > T	p.(Arg368Cys)	R329C /
155206167	C	T	c.1093G > A	p.(Glu365Lys)	E326K /
155206172	A	G	c.1088T > C	p.(Leu363Pro)	L324P /
155207329	C	T	c.802G > A	p.(Ala268Thr))	A229T /
155207367	A	T	c.764T > A	p.(Phe255Tyr)	F216Y /
155207932	A	C	c.754T > G	p.(Phe252Val)	F213V /
155207985	C	T	c.701G > A	p.(Gly234Glu)	G195E /
155208361 155206167	C A	G G	c.535G > C c.1093G > A	p.[(Asp179His; Glu365Lys)]	D140H + E326K /
155208421	G	A	c.475C > T	p.(Arg159Trp)	R120W
155210482	TA	T	c.53delT	p.(Val18fs)	V-21fs
155206167 155206167	C C	T T	c.1093G > A c.1093G > A	p.[(Glu365Lys)]; [(Glu365Lys)]	E326K / E326K
Synonymous					
155206117	A	G	c.1143T > C	p.(Cys381=)	C342= /

Protein coordinated (pNomen) are presented according to NP_000148.2. Common variant name historically used (Allelic name) is presented after removing the 39 aa signal sequence. Protein coordinates of the variant according to NP_000148.2. rsID = Reference SNP ID assigned by dbSNP or EVA. Clinical significance of the variant (Label-denHeijer) is presented as previously reported in [32] (GD = Gaucher Disease, PD = Parkinson's Disease). aa = amino acid.

Known and novel GBA1 variants in a Dutch postmortem cohort of PD, iLBD and Controls

In the 160 postmortem brains of the *genotyping cohort* sequenced for *GBA1* (Table 1) we detected 70 unique variants, 47 single-nucleotide polymorphisms (SNPs) and 23 insertions/deletions, yielding a mean of 10 ± 4 variants per individual. The variants of interest identified (exonic or within ± 5 bp from canonical splice site; see Material and Methods) are presented in Supplementary Table 1 (see Suppl. File 1). Among these, we confirmed 9 known PD-associated heterozygous variants: N370S (n = 2), T369M (n = 4), R329C (n = 1), E326K (n = 7), L324P (n = 1), F216Y (n = 1), F213V (n = 1), G195E (n = 1), R120W (n = 1), L383fs (n = 1), A229T (n = 1) [30, 32, 89–93]. The E326K was the most common *GBA1* variant (4.4% of PD cases), as previously reported in the Dutch PD population [32]. The variant E326K was also identified in a homozygous configuration (E326K / E326K; n = 1). The variant D140H was identified in a combined configuration with E326K (D140H + E326K /; n = 3), as previously described specifically in the Dutch population (Dutch founder variant) [32]. We also describe the frameshift *GBA1* variant V-21fs (n = 1), not previously reported, expanding the known mutational spectrum of *GBA1*. A synonymous substitution, C342=

(n = 1), was identified in a PD case. Overall, 25 of 114 PD brains (21.9%) carried a deleterious missense variant and one (0.9%) harboured a synonymous change, whereas only one missense carrier was found among 21 neuropathologically normal controls (D140H + E326K /; 4.8%). Remarkably, no *GBA1* variants of interest were identified in the iLBD group (0/25).

Comparison of clinical and pathological profiles between PD *cases with and without GBA1 variants.*

Next, we compared the clinical information between the IPD and the GBA-PD cases in the *biochemistry cohort* (Suppl. Figure 7). Median age at death, age at motor symptoms onset and overall disease duration were each slightly lower in the GBA-PD group than in the IPD group; however, none of these differences reached statistical significance. The interval between motor onset and the emergence of dementia displayed a similar non-significant trend toward a shorter interval in GBA-PD. Hallucinations were more prevalent in carriers: 90% of GBA-PD patients reported visual hallucinations compared with 72% of IPD patients (p = 0.020). Finally, *GBA1* variants were more frequent in PDD than in PD without dementia (68% versus 50%), but this did not achieve statistical significance (Fisher's exact test, p = 0.20).

Regional and fraction-specific αSyn proteoforms distribution in controls, iLBD and PD

We next compared the levels and solubility of αSyn proteoforms across PD, iLBD and control cases (Fig. 2). Using sequential protein extraction of the LC, SN and GTM, we generated a RIPA-soluble fraction ("Soluble") and a RIPA-insoluble/UTC-soluble fraction ("Insoluble"), in which we quantified Total, pSer129 and CTT122 αSyn by alphaLISA (Fig. 1; Suppl. Figure 2). In all cases, median Soluble Total αSyn concentrations differed markedly by region, extending from 268 pG/mG in the LC, 765 pG/mG in the SN, to 3034 pG/mG in the GTM (Fig. 2a). Across all cases and regions, the median Soluble pSer129 αSyn was two to three orders of magnitude lower compared to Total αSyn, ranging between 0.7–5.4 pG/mG (Fig. 2b), while median Soluble CTT122 αSyn ranged between 0 and 163 pG/mG (Fig. 2c) in the three brain areas. Thus, within the Soluble pool, pSer129 and CTT122 αSyn constituted less than 0.3% and 5.4% of Total αSyn, respectively. For all quantified Soluble αSyn proteoforms, levels were lowest in the LC, higher in the SN, and further increased in the GTM (Fig. 1a-c). For Soluble Total αSyn, median level in all cases rose by 2.9-fold in SN and 11.3-fold in GTM relative to LC. Soluble Total, pSer129 and CTT122 αSyn concentrations were largely comparable between groups in all three regions, except for Soluble Total αSyn in the SN which was lower in PD brains (-39% versus controls, p = 0.003; -48% versus iLBD, p = 0.003), and for Soluble pSer129 αSyn showing a modest but significant increase in the LC of PD cases (+ 28% versus controls, p = 0.041).

In the Insoluble fraction, we observed substantial differences between groups. Insoluble Total αSyn was significantly elevated in LC of PD brains, rising by 173% versus controls and 80% versus iLBD (both p < 0.001; Fig. 2d). We observed a parallel upward trend compared to controls in SN (iLBD: +34%; PD: +38%) and GTM (iLBD: +29%; PD: +60%) of both iLBD and PD groups, which did not reach significance. Overall, the levels of Insoluble Total αSyn were comparable between regions in all cases (median ~ 143 pG/mG). By contrast, Insoluble pSer129 αSyn was undetectable in any region of control cases (median in all areas = 0 pG/mG) but increased sharply in PD (LC: 23.5; SN: 15.4; GTM: 4.48 pG/mG; all p < 0.001 vs controls; Fig. 2e). Notably, median Insoluble pSer129 αSyn was also increased in iLBD compared to controls in LC, SN and GTM (in iLBD: LC = 0.93; SN = 7.06; GTM = 0 pG/mG; all p < 0.001 vs controls).

In PD cases, the increase of median Insoluble pSer129 relative to controls was greatest in LC (23.5 vs 0 pG/mG, p < 0.001), diminished in SN (15.4 vs 0 pG/mG, p < 0.001), and further reduced in GTM (4.48 vs 0 pG/mG, p < 0.001). When comparing Insoluble αSyn levels between the three brain regions in all cases, median pSer129 αSyn levels were lower in SN and further decreased in GTM compared to LC (from 7.2 in LC to 1.5 pG/mG in GTM), which was the opposite of what observed in Soluble pSer129 αSyn.

For the Insoluble CTT122 αSyn quantification, we observed a high number of cases with no detectable protein, which were less prevalent in the iLBD and PD groups compared to controls. The amount of Insoluble CTT122 showed substantial variability in all groups (Fig. 2f). In all brain regions we observed an overall trend towards increased Insoluble CTT122 levels in iLBD compared to controls, although this did not often reach significance. We observed a statistical significant increase in the PD vs control (LC: 49.7 vs 14.8 pG/mG, p < 0.001; SN: 25.8 vs. 0 pG/mG, p < 0.001; GTM: 0 vs. 0 pG/mG, p < 0.001; median) and vs iLBD (LC: 49.7 vs 20.2 pG/mG, p < 0.001; SN: 25.8 vs 18.6 pG/mG, p = 0.042.; GTM: 0 vs 0 pG/mG, p < 0.001; median). These differences were more marked in the LC and progressively decreased in SN and GTM. Overall, the total amount of Insoluble pSer129 and CTT122 αSyn was lower than the protein recognized by the Total αSyn assay in all cases (Total: 108.2-195.7; pSer129: 1.4–7.2; CTT122: 0-25.6 pG/mG; median range), representing about 0.7–6.7% (for pSer129 αSyn) and 0-23.7% (for CTT122 αSyn) of measured Total αSyn protein.

To identify the biochemical measure that could best predict the presence of Lewy pathology (LP) in iLBD and PD, we compared the diagnostic performance of every available read-out (Total, pSer129, and CTT122 αSyn in Soluble and Insoluble fractions) together with all derived ratio permutations by quantifying the area under the receiver-operating-characteristic curve (ROC AUC) (Fig. 2g; Suppl. File 3). Across all candidate metrics, the ratio of Insoluble pSer129 to Soluble Total αSyn yielded the highest composite performance (product of regional AUCs; Suppl. File 2), with a mean sensitivity of 88%, mean specificity of 82% (at > 0.072 pG Insol. pSer129/pG Total Sol.; Suppl. File 2) and with a mean AUC = 0.87 for distinguishing controls from cases with LP. The next-best performers were the ratio of Insoluble pSer129 to Insoluble Total αSyn and the absolute level of Insoluble pSer129 alone. Together, the data indicate Insoluble pSer129 as the single most informative biochemical marker of αSyn pathology in the brain, with normalization to Soluble Total αSyn further enhancing diagnostic power. Accordingly, all subsequent analyses employ the *Insoluble pSer129/Soluble Total αSyn* ratio (hereafter termed *pSer129 αSyn ratio*; Fig. 2h).

To investigate inter-relationships among αSyn proteoforms, we computed all pair-wise Spearman correlations for Total, pSer129, and CTT122 αSyn within the LC, SN, and GTM in both Soluble and Insoluble fractions (Fig. 3a). No significant association emerged in any readout between in the Soluble and Insoluble measures, and proteoform levels in one region did not correlate with those in another (p > 0.05 for every cross-fraction or cross-region comparison). By contrast, the three Insoluble species were tightly inter-related within each region (Spearman r ranged from 0.49 to 0.93 across the LC, SN, and GTM; all p < 0.001) (Fig. 3b–d). The Soluble pool showed a more limited pattern as only Total and pSer129 αSyn pairs showed significant correlation with CTT122 in SN

and GTM, with moderate effect sizes (r = 0.29–0.61, all p < 0.05; Fig. 3a). Collectively, these data indicate that Soluble and Insoluble αSyn reservoirs behave independently in postmortem brain, whereas the Insoluble fraction maintains tight, region-restricted relationships among the αSyn proteoforms measured.

Table 3

α-synuclein protein levels, glucocerebrosidase activity, and glucocerebrosidase protein levels in postmortem PD and iLBD brain tissue. α-synuclein (αSyn) protein levels are expressed as median pG of αSyn per mG of total protein. Glucocerebrosidase (GCase) activity is expressed as median mol of product per hour per mG of total protein. GCase protein levels are expressed as median pG per mG of total protein. Change from the control group (CTRL) is reported as fold change expressed as percentage increase/decrease (% FC vs CTRL). Ins. = Insoluble UTC fraction; CI = 95% confidence interval; CTRL = control cases; iLBD = incidental Lewy body disease cases; IPD cases = idiopathic Parkinson's disease (PD) cases; GBA-PD = PD cases with *GBA1* risk variants; □ = IPD.

CTRL	Ins. Total αSyn levels Median pG/mG; CI (% FC vs CTRL)	Ins. pSer129 αSyn levels Median pG/mG; CI (% FC vs CTRL)	Ins. CTT122 αSyn levels Median pG/mG; CI (% FC vs CTRL)	GCase activity Median mol/hr/mG; CI (% FC vs CTRL)	GCase levels Median pG/mG; CI (% FC vs CTRL)
	LC: 57.7 ; 36.4–78.0 **(-)** **SN: 121; 52.8–127** **(-)** **GTM: 131; 102–177** **(-)**	**LC: 0.00; 0.00–0.00** **(-)** **SN: 0.00; 0.00–0.00** **(-)** **GTM: 0.00; 0.00–0.00** **(-)**	**LC: 12.1; 0.00–18.6** **(-)** **SN: 0.00; 0.00–6.38** **(-)** **GTM: 0.00; 0.00–0.00** **(-)**	**LC: 7.24; 7.05–7.82** **(-)** **SN: 7.39; 6.31–8.20** **(-)** **GTM: 8.16; 7.65–9.13** **(-)**	**LC: 12.3; 10.2–13.2** **(-)** **SN: 20.4; 17.4–22.9** **(-)** **GTM: 18.6; 17.2–19.3** **(-)**
iLBD	**LC**: 85.5 ; 44.4–99.0 (+ 48%) **SN**: 149; 111–204 (+ 23%) **GTM**: 177; 134–242 (+ 34%)	**LC**: 0.862; 0.319–6.17 (+∞) **SN**: 4.35; 0.00–12.6 (+∞) **GTM**: 0.00; 0.00–0.00 (+∞)	**LC**: 20.9; 15.6–25.8 (+ 72%) **SN**: 17.8; 0.00–25.2 (+∞) **GTM**: 0.00; 0.00–0.00 (-)	**LC**: 7.06; 6.39–8.02 (-3.6%) **SN**: 7.02; 6.21–7.79 (-5%) **GTM**: 8.33; 7.54–8.91 (+ 2%)	**LC**: 11.5; 9.94–12.9 (-7%) **SN**: 17.4; 14.8–19.2 (-15%) **GTM**: 18.3; 17.0–19.4 (-2%)
IPD (□)	**LC**: 126 ; 88.9–191 (+ 119%) **SN**: 159; 113–211 (+ 32%) **GTM**: 214; 162–250 (+ 63%)	**LC**: 18.4; 5.62–37.6 (+∞) **SN**: 12.3; 4.76–25.0 (+∞) **GTM**: 4.93; 2.66–11.0 (+∞)	**LC**: 46.4; 25.4–56.7 (+ 282%) **SN**: 29.1; 17.5–39.0 (+∞) **GTM**: 8.16; 0.00–13.5 (+∞)	**LC**: 6.79; 6.07–7.56 (-6.2%) **SN**: 5.79; 5.27–6.94 (-21.6%) **GTM**: 8.16; 7.91–8.63 (0%)	**LC**: 10.4; 9.12–12.0 (-16%) **SN**: 14.6; 12.8–16.1 (-28%) **GTM**: 18.0; 16.7–20.0 (-3%)
GBA-*PD*	**LC**: 162 ; 149–196 (+ 181%; +29% vs □) **SN**: 248; 136–352 (+ 105%; +55% vs □) **GTM**: 215; 139–239 (+ 64%; 0% vs □)	**LC**: 24.2; 20.9–33.9 (+∞; +32% vs □) **SN**: 25.3; 12.8–31.7 (+∞; +106% vs □) **GTM**: 4.29; 1.89–11.7 (+∞-; -13% vs □)	**LC**: 52.6; 44.7–59.0 (+ 333%; +13% vs □) **SN**: 47.4; 25.6–53.1 (+∞; +63% vs □) **GTM**: 0.00; 0.00–14.6 (-; -100% vs □)	**LC**: 4.03; 3.43–4.15 (-44%; -41% vs □) **SN**: 4.36; 2.99–5.89 (-41%; -25% vs □) **GTM**: 5.28; 4.96–6.26 (-35%; -35% vs □)	**LC**: 10.3; 7.57–12.3 (-16%; -1% vs □) **SN**: 12.7; 11.3–16.8 (-38%; +13% vs □) **GTM**: 15.6; 15.0–16.0 (-16%; -13% vs □)

pSer129 αSyn in GBA1 and idiopathic PD

To examine whether the presence of *GBA1* variants modulates αSyn pathology, we compared the *pSer129 αSyn ratio* between GBA-PD and IPD cases across the LC, SN, and GTM (Fig. 4a). While higher *pSer129 αSyn ratio*s were found in GBA-PD than in IPD in the LC (+ 25%,) and SN (+ 39%), these differences were not statistically significant. No elevation was detected in the GTM (-5.2%, n.s.). The *pSer129 αSyn ratio* was increased in IPD cases compared to controls (all p < 0.005) and iLBD (all P < 0.05), as well as in iLBD cases versus controls in LC and SN (all p < 0.005). To test for differences between groups irrespective of anatomical area, we modelled the *pSer129 αSyn ratio*s across groups in all areas (GLMM with anatomical region as covariate, see Material and Methods). No significant difference between IPD and GBA-PD was observed. We then stratified GBA-PD cases by *GBA1* variant severity (see Materials and Methods) to evaluate whether severe alleles associate with greater αSyn accumulation (Fig. 4b–d). Neither the *pSer129 αSyn ratio* nor any individual αSyn proteoform varied across *GBA1* variant severity classes, and no consistent trend emerged. Of note, the case carrying the V-21fs variant showed high *pSer129 αSyn ratio* (LC: 92.1; SN: n.a.; GTM: 4.3 pG/mG). PD cases carrying the E326K variant had similar *α*Syn load compared to IPD cases (p = 0.396 in all areas). Details on αSyn proteoforms levels measured in this study are presented in Table 3.

GCase deficiency in PD and iLBD

To determine whether PD and iLBD cases show GCase deficiency, we quantified total GCase enzyme activity (GCase activity) and GCase protein levels in the LC, SN, and GTM of control, iLBD, IPD, and GBA-PD cases (Fig. 5a). As expected, GBA-PD cases showed a pronounced GCase activity reduction relative to controls in every region (LC: -44%, $p < 0.001$; SN: -41%, $p < 0.001$; GTM: -35%, $p < 0.001$) and also relative to both iLBD (LC: -43%, $p < 0.001$; SN: -38%, $p = 0.001$; GTM: -37%, $p < 0.001$) and IPD (LC -41%, $p < 0.001$; SN:-25%, $p <= 0.005$; GTM: -35%, $p < 0.001$). In iLBD and IPD, GCase activity was lower than controls in LC (iLBD: -2.4%; IPD: -6.2%) and SN (iLBD: -5%; IPD: -21.6%), but these trends did not reach significance. GCase activity measures in iLBD and IPD were similar to controls in the GTM. Importantly, when modelling GCase activity across disease groups to test for differences irrespectively of anatomical area (GLMM with anatomical region as covariate, see Material and Methods), IPD showed reduced GCase activity overall compared to controls (-11%, $p = 0.044$), effect not evident in single-region analyses. Median GCase activity in controls was not different between anatomical regions (range: 7.2–8.2 µmol/hr/mG).

Total GCase protein levels partially mirrored the GCase activity results across diagnostic groups, with good correlation between GCase activity and GCase protein levels (LC: $R = 0.17$, $p = 0.16$; SN: $R = 0.56$, $p < 0.001$; GTM: $R = 0.35$, $p < 0.001$; Fig. 5b; Suppl. Figure 9). Of note, both iLBD, IPD and GBA-PD showed diminished GCase abundance relative to controls in the SN (iLBD:-14.8%, $p = 0.095$; IPD: -28.4%, $p = 0.025$; GBA-PD: -37.5%, $p = 0.003$). The GCase levels in LC were reduced in all groups compared to controls, but this difference did not reach significance (iLBD:-6.6%, p = n.s.; IPD: -15.8%, p = n.s.; GBA-PD: -16.2%, p = n.s.) In the GTM, only GBA-PD levels were significantly decreased (iLBD:-1.8%, p = n.s.; IPD: -3.2%, p = n.s.; GBA-PD: -16.0%, $p = 0.012$). Across controls, GCase protein levels were higher in SN and GTM compared to LC (+ 65% and + 51%, respectively). To investigate changes in specific catalytic activity from protein abundance, we normalised activity to GCase protein (GCase specific activity; Fig. 5c). In controls, specific activity was lower in SN and GTM than in LC (-36% and − 26%, respectively; $p < 0.005$). Interestingly, specific activity did not show a significant difference in iLBD and IPD compared to controls, but was significantly reduced in GBA-PD in LC (-36%, $p = 0.004$) and GTM (LC: -36%, $p = 0.004$; SN: -21.9%, p = n.s.; GTM: -18%, $p < 0.001$), and versus IPD in SN (-39.5%, $p = 0.043$). Specific activity negatively correlated with variant severity (see *Material and Methods*) in PD cases in all areas (Spearman's $\rho \leq -0.50$, $p \leq 0.05$ in all areas), as expected (Suppl. Figure 8). Details on GCase activity, GCase protein levels, and GCase-specific activity measured in this study are presented in Table 3.

To assess whether GCase function associates with *GBA1* variant severity, we stratified PD brains into mild, intermediate, and severe allele groups and compared their enzyme activities with those of IPD (Fig. 5d–f; see *Materials and Methods*). GCase activity declined stepwise from mild to intermediate and severe carriers in the LC and GTM; however, none of these pairwise differences reached statistical significance, possibly due to the small number of cases per group. Nonetheless, GCase activity and variant severity correlated (LC: $\rho = 0.77$, $P < 0.001$; SN: $\rho = 0.37$, $p = 0.09$; GTM: $\rho = 0.75$, $p < 0.001$). The case carrying the V-21fs variant displayed low levels of GCase activity in both LC and GTM (LC: 3.4; SN: n.a.; GTM: 5.18 µmol/hr/mG). PD cases carrying the E326K variant had decreased GCase activity compared to IPD cases (-60.2 ~ 18.7%; $p < 0.005$ in all areas).

GCase activity correlates negatively with αSyn levels

We then examined the correlation between *pSer129 αSyn ratio* and GCase activity in GBA-PD, IPD and iLBD within each region (Fig. 6). Pearson analysis showed a robust inverse correlation in LC ($r = -0.32$, $p = 0.007$) and SN ($r = -0.59$, $p < 0.001$). In the GTM, however, no significant correlation was found ($r = -0.13$, p = n.s.). Interestingly, when analysing the correlation in the IPD group alone, we also observed a significant correlation between *pSer129 αSyn ratio* and GCase activity in the LC and SN (LC: r=-0.59, $p = 0.028$; SN: r=-0.61, $p = 0.016$), which was not significant in the GTM (r=-0.23, $p = 0.155$). Overall, these results suggest an association between reduced GCase activity and the accumulation of Insoluble αSyn proteoforms bot the presence and absence of *GBA1* risk variants.

Clinical and neuropathological correlates of regional pSer129 αSyn levels

We next asked whether regional αSyn pathology correlates with clinical variables in the PD cohort (Fig. 7). Stratifying cases by short versus long disease duration (compared to median: < 15 vs ≥ 15 years; Fig. 7a) or early versus late disease onset (compared to median: < 62 vs ≥ 62 years; Fig. 7b) revealed no significant differences in the LC, SN, or GTM, apart from a modest increase in *pSer129 αSyn ratio* in the LC of early-onset cases ($p = 0.047$). In contrast, a sex effect was found: females displayed substantially lower pSer129 αSyn ratios than males in the LC (-67%, $P = 0.004$), while GTM and SN values were comparable (Fig. 7c).

Comparing PD cases based on the presence of dementia showed that PD cases with dementia (PD + D) had a 143% increase in the *pSer129 αSyn ratio* in the GTM relative to PD without dementia (PD − D; $p = 0.003$). No differences were observed in the brain-stem areas (Fig. 7d), suggesting specific increase in cortical pathology in PD cases with dementia. Finally, across all cases, the *pSer129 αSyn ratio* correlated strongly with Braak αSyn stage in every region (LC: $\rho = 0.73$, $p < 0.001$; SN: $\rho = 0.74$, $p < 0.001$; GTM: $\rho = 0.70$, $p < 0.001$; Fig. 7e-g), underscoring a link between Insoluble pSer129 αSyn biochemical levels and anatomical disease progression.

Clinical and neuropathological correlates of GCase enzyme activity in PD

We next examined whether total GCase activity associated with disease duration, age at onset, sex, presence of dementia and Braak stage (Fig. 8). GCase activity did not differ between cases with short versus long disease duration (compared to median: < 15 vs ≥ 15 years), between early- and late-onset groups (compared to median: < 62 vs ≥ 62 years), nor between males and females (Fig. 8a–c). Likewise, PD + D and PD − D cases displayed comparable enzyme activity in all three regions (Fig. 8d). By contrast, GCase activity was inversely correlated with Braak αSyn stage (LC: $\rho = -0.40$, $p < 0.001$; SN: $\rho = -0.37$, $p = 0.006$; GTM: $\rho = -0.30$, $p < 0.001$; Fig. 8e–g), indicating that progressive increase in neuropathological staging is accompanied by gradually diminishing GCase hydrolase function. Nonetheless, this correlation was not significant when excluding the GBA-PD cases from the analysis (LC: $\rho = -0.19$, $p = 0.191$; SN: $\rho = -0.30$, $p = 0.054$; GTM: $\rho = -0.02$, n.s.).

Discussion

Our comprehensive quantitative analysis of postmortem human brain provides a region-resolved biochemical profile of the relation between αSyn accumulation and GCase deficiency in iLBD, GBA-PD and IPD. By pairing immunoassays with enzymology, we provide a readout of the absolute concentration of Total, pSer129 and CTT122 αSyn together with GCase total activity, protein abundance, and specific activity in the brain-stem nuclei (LC and SN) and the cortex (GTM). Full-length *GBA1* sequencing uncovered one previously unreported variant, expanding the mutational landscape of PD. Insoluble pSer129 and CTT122 αSyn were markedly elevated in iLBD, GBA-PD and IPD relative to controls while Insoluble αSyn proteoforms did not differ between GBA-PD and idiopathic cases in our cohort. This data do not support an increased cortical involvement in PD pathology of *GBA1* risk variant carriers compared to idiopathic, as previously reported [35, 36]. *GBA1* variant severity failed to stratify αSyn burden. In contrast, GCase catalytic activity was sharply reduced in GBA-PD. In IPD, the observed reduction of GCase activity showed a statistically significant reduction overall when modelling all anatomical areas together. GCase protein abundance dropped in both GBA-PD and IPD only in the SN. Normalising activity to protein revealed a selective loss of GCase specific activity only in *GBA1* carriers, implying that the apparent deficit in idiopathic disease is driven primarily by reduced enzyme quantity. Crucially, pSer129 αSyn levels inversely correlated with GCase activity in both IPD and GBA-PD. Collectively, our data highlights GCase dysfunction a biochemical correlate of aggregated αSyn in both genetic and idiopathic synucleinopathies.

Full sequencing of *GBA1* in 160 Dutch brain donors showed missense variants in 21.9% of PD cases (n = 114). A prospective study in living Dutch patients reported variants in 15% of PD cases, demonstrating the high prevalence of *GBA1* variants in the Dutch population compared to other populations [30, 32]. The higher frequency we observed likely reflects the use of postmortem brain selected on neuropathologically-confirmed PD and PDD cases after death, rather than on clinically diagnosed PD patients, which include misdiagnoses. A study in the Dutch population showed that 8.5% of cases clinically diagnosed with PD, did not have clinical parkinsonism after clinical re-evaluation [94]. Moreover, several studies have demonstrated the low diagnostic accuracy of clinical PD diagnosis after validation by postmortem neuropathological assessment [95–97]. 15% of cases diagnosed with clinical PD did not show LP after neuropathological examination in the Dutch population [98]. Thus, our measurement in neuropathologically-confirmed PD cases might be a more accurate estimation of the prevalence of *GBA1* variants in true PD cases in the Dutch population.

Biochemical profiling showed a marked increase in αSyn only in the Insoluble fraction of PD and iLBD brains, while the Soluble pool was largely unchanged. This confirms the finding that disease-associated αSyn accumulation is composed of aggregated, detergent-insoluble assemblies rather than of soluble and non-aggregated αSyn protein, consistent with an earlier postmortem study [23]. This suggests the conversion of protein to insoluble forms, rather than just the increase in total syn levels, to be the main pathological mechanism in synucleinopathies. In recent perspectives by Espay et al., an alternative theory was presented in which the loss of monomeric αSyn (synucleinopenia) is the key pathogenic mechanism in the disease, rather than aggregated insoluble αSyn [99, 100]. Our data however suggests otherwise, as soluble αSyn was largely unchanged in the Soluble fraction, both in PD and iLBD (Fig. 2). The reduction observed by us in the Soluble fraction in the Total αSyn readout in the SN of PD cases could be explained by the neuronal loss observed in this region. No reduction was observed in the iLBD group. Additionally, no correlation was observed in αSyn protein levels between the Soluble and Insoluble fractions (Fig. 3). All PD-related αSyn changes were observed only in the Insoluble fraction, which strongly correlated with Braak staging (Fig. 7). Overall, these do not indicate the reduction of monomeric αSyn (loss-of-function) as pathogenic mechanism in PD. Moreover, the absence of the accumulation of soluble αSyn may reflect the rapid conversion of excess αSyn into higher order species, or indicate that insoluble deposits represent a terminal step in αSyn catabolism.

Our analysis in different brain regions revealed that insoluble αSyn was highest in the LC, lower in the SN, and lowest in the GTM, potentially mirroring the caudo-rostral spread of LP in PD, despite differences in neuronal density [1]. Similarly, Total Soluble αSyn was overall higher in SN and further elevated in the GTM overall compared to LC, possibly reflecting difference in the abundance of neurons/synapses. Most of the changes between the diagnostic groups were observed in the Insoluble fraction in the pSer129 and CTT122 proteoforms, rather than in the Total αSyn assay. This, together with the observation that pSer129 αSyn is low and unchanged in the Soluble fractions (and virtually absent in the Insoluble fraction of the control group), indicates that most aggregated pathological αSyn protein is phosphorylated at Ser129, which aligns with previous findings [101–103]. This is further confirmed by the lack of correlation between measurements in the Soluble and Insoluble fractions (Fig. 3). Overall, our data might suggest Ser129 phosphorylation and CTT122 as post-aggregation modifications, which is supported by the observation that pSer129 and CTT122 αSyn constituted a small percentage of Total Soluble αSyn (0.3 and 5.4% respectively). Moreover, this is in line with our microscopic data showing pSer129 and CTT122 αSyn primarily in neuronal inclusions [7, 104]. Together, these findings in both PD and iLBD, confirm pSer129 αSyn, and especially the ratio between Insoluble pSer129 and Soluble Total αSyn, as specific molecular biomarker for PD in human brain. Moreover, this strongly indicates the importance of sequential protein extraction when evaluating αSyn load as a biomarker in brain and, possibly, in other biofluids.

When comparing αSyn levels in the GBA-PD group we observed a slight non-significant increase in LC and SN compared to IPD, and no difference in cortical GTM. Given previous report of increased pathology and increased involvement in cortical areas in GBA-related parkinsonism, we expected an increase in αSyn levels in this group, which was not observed [37, 39]. This suggests that GBA-related parkinsonism does not invariably associate with increased αSyn pathology in the cortex, which is in line with recent studies [42, 43, 105]. For example, Parkinen et al. quantified LB density in several cortical regions in PD cases, including temporal cortex, and showed no difference between cases with and without *GBA1* variants [42]. Furthermore, our comparison of Insoluble αSyn levels between PD cases with different *GBA1* variant severity did not identify any difference between cases without *GBA1* variants and cases with mild, intermediate, or severe *GBA1* variants in any of the brain regions analysed. Nonetheless, we observed an inverse correlation between GCase activity and Insoluble pSer129 αSyn levels. As in our analysis total GCase activity correlated poorly with variant severity (see Fig. 5d-f), this might suggest that additional factors are at play in determining total GCase activity. This becomes apparent in cases carrying frameshift variants, which only carry one functioning copy of *GBA1*, which displayed GCase activities comparable to other IPD or GBA-PD cases, suggesting the existence of complementary mechanisms.

When measuring GCase activity, we observed a marked reduction in the GBA-PD group compared to controls, which was the highest in LC, lower in SN and further reduced in GTM. This also followed the temporal involvement of these areas according to Braak anatomical αSyn spreading model [1]. Regarding IPD,

we only found non-significant negative trends in LC and SN. This is in accordance with previous report in frontal cortex [44]. Many studies attempted at identifying a difference between IPD and controls, which was often minor and mostly not significant [38, 44, 105–107]. The lack of statistical significance might be due to the combination of high variability among cases and to the subtlety of the change observed. Importantly, this reduction was significant in our data when modelling all anatomical areas at once, indicating that GCase activity is indeed reduced in IPD compared to controls overall. Moreover, we describe the existence of a strong negative correlation between GCase activity and *α*Syn levels in the IPD group alone. Overall, these data indicate that GCase dysfunction associates with Insoluble αSy accumulation in PD independently of *GBA1* status.

We also observed reduced GCase protein levels in GBA-PD (in SN and GTM) and IPD (in SN), in accordance to what previously reported in idiopathic PD in the anterior cingulate cortex [39]. Normalization of GCase activity on the amount of GCase protein showed a reduction in specific enzyme activity in the GBA-PD group, as expected, but not in the IPD group. This indicates that the observed reduction of GCase activity in the IPD group might be due to a reduction in enzyme levels, suggesting the GCase enzyme is functional but its levels are reduced. These results may indicate difference mechanisms underlaying GCase dysfunction in GBA-PD and IPD. GCase expression, activation or degradation might be altered in IPD, in association with αSyn accumulation, while, in GBA-PD, GCase impairment might be due to a reduction in specific enzymatic activity due to the presence or variants. Accordingly, a reduction of GCase activity has been reported in the cerebellum in GBA-PD/PD, area which is largely unaffected by αSyn pathology [105]. The hypothesis that GCase dysfunction might happen in response to αSyn accumulation in IPD, while it could be a result of underlying GCase impairment in GBA-PD, is in line with the proposed bidirectional pathogenic loop between GCase and αSyn [48]. Thus, GBA-cases might have additional susceptibility to initial αSyn accumulation, but similar regional pathological progression. Differently, αSyn accumulation in the IPD might be a result of underlying low-level GCase impairment. In both hypothesis, this leads to similar levels of accumulated αSyn between IPD and GBA-PD, as demonstrated in this study (Fig. 4a). Further mechanistic studies are needed to elucidate the differences between IPD and GBA-PD disease mechanisms.

Limitations of this study include the use of postmortem brain tissue, which hinders causal/temporal interpretation of results, and the limited availability of tissue in some areas (especially in SN) and in GBA-PD cases, which is also partially due to the rarity of GBA-PD cases. This has limited the statistical power in some analysis, especially when looking at different GCase variant severity. Another limitation is that the ELISA assay used in this study to measure GCase levels was based on antibodies for which the target epitope is unknown. Thus, the measurements in cases carrying certain variants might be influenced by the different affinity of the ELISA's antibodies due to the presence of a different amino acid at, or near, their binding site. A key advantage of the present study is its fully quantitative biochemical workflow using high throughput absolute αSyn proteoform concentrations (Total, pSer129, CTT122) and GCase kinetics (total activity, protein abundance, specific activity) with calibrated immunoassays and enzymology. Combined with a four-arm cohort spanning controls, iLBD, IPD and GBA-PD, severity-graded *GBA1* subgroups, and tri-regional sampling (LC, SN, GTM), this design delivers a region-resolved depiction of the αSyn-GCase axis.

In conclusion, our findings underline a biochemical link between aggregated, pSer129-enriched αSyn pathology and GCase deficiency across clinical and preclinical PD spectrum in both GBA-related and idiopathic PD, underscoring lysosomal dysfunction as a central feature of the disease. This highlights the potential benefit of therapies aimed at boosting GCase activity or otherwise restoring lysosomal function, which could help attenuate αSyn accumulation in both IPD and GBA-PD. Notably, we observed no evidence of increased cortical αSyn pathology in GBA-associated PD, indicating that while *GBA1* variants heighten the risk of PD, may not fundamentally alter the degree and pattern of αSyn deposition. The study also underlines possible differences in disease mechanism between GBA-PD and IPD. Longitudinal studies in clinical PD cohorts, ideally stratified by *GBA1* status, will be essential to guide precision therapies aimed at restoring the αSyn-GCase balance potentially and slowing disease progression.

Declarations

Ethical approval and consent to participate

Postmortem human brain tissue was collected from clinically diagnosed and neuropathologically verified donors with PD, PDD, iLBD, and non-demented controls by the NBB and CNAB. Informed consent for brain autopsy and the use of brain tissue and clinical information for scientific research was obtained from either the donor or their next of kin, in accordance with all local ethical and legal guidelines. The NBB's Code of Conduct and Ethical Declaration is publicly accessible to ensure compliance with these standards [55, 56, 108]. All procedures were approved by the Institutional Review Board and Medical Ethical Board (METC) of the Amsterdam UMC, Amsterdam.

Financial disclosure

W.D.J.vd.B. received financial support from the Michael J. Fox foundation (U.S.A; MJFF-009210; MJFF-022468) and Stichting Woelse Waard (The Netherlands; ParkCode) for this study. V.B. received financial support from the Stichting Parkinson Fonds (The Netherlands; Grant. n. 1880).

Competing interests

The authors declare that they have no competing interests. M.L.M., T.E.M., H.G., M.B. and V.U. are or were full-time employees of Roche/F. Hoffmann-La Roche Ltd. and may additionally hold Roche stock/stock options. W.D.J.vd.B. is a member of the scientific advisory board of Gain Therapeutics, a member of the scientific board of Alzheimer Nederland, and the president of the Dutch Parkinson scientists association.

Author Contribution

M.L.M. ideated the project, designed experiments, executed experiments, analysed data, wrote the manuscript and contributed to patient selection. M.T. and J.J.P.B. performed experiments. F.F. and L.P. analysed data and contributed to manuscript preparation. T.E.M., V.U. and V.B. contributed to manuscript preparation. M.B. contributed to experiment design. W.A.B. contributed to experiment design and executed experiments. A.M.T.I. performed experiments, contributed to tissue handling and manuscript preparation. H.G. contributed to patient selection. W.D.J.vd.B. ideated the project, contributed to experimental design, patient selection and to manuscript preparation.

Acknowledgement

We thank all the brain donors and their families for their donation. We would also like to thank the NBB, CNAB and their autopsy team. We thank Thecla van Wageningen, Irene Frigerio, Laura E. Jonkman, Evelien Timmermans, John J. Bol, Allert Jonker, Zilan Ayhan (Amsterdam UMC, department of Anatomy and Neurosciences, Amsterdam, The Netherlands) for the help with patient selection, tissue handling, and with the processing of clinical and neuropathological information. We thank Steven J. Roeters and Bram van der Gaag (Amsterdam UMC, Vrije University Medical Center, department of Anatomy and Neurosciences, Amsterdam, The Netherlands) for the help with the development of the alphaLISA assays. We also thank Markus Britschgi (Roche Pharma Research and Early Development, Neuroscience and Rare Diseases Discovery and Translational Area, Roche Innovation Center, Basel, Switzerland) for the scientific exchange and for providing the primary antibodies against pSer129 (Syn-142) and for the truncated recombinant αSyn proteins.

Data Availability

The datasets supporting the conclusions of this article are included within the article and its additional files.

References

1. Braak, H., et al., *Staging of the intracerebral inclusion body pathology associated with idiopathic Parkinson's disease (preclinical and clinical stages)*. J Neurol, 2002. 249 Suppl 3: p. III/1–5.
2. Spillantini, M.G., *Parkinson's disease, dementia with Lewy bodies and multiple system atrophy are alpha-synucleinopathies*. Parkinsonism Relat Disord, 1999. 5(4): p. 157–62.
3. Spillantini, M.G., et al., *Alpha-synuclein in Lewy bodies*. Nature, 1997. 388(6645): p. 839–40.
4. Spillantini, M.G., et al., *alpha-Synuclein in filamentous inclusions of Lewy bodies from Parkinson's disease and dementia with lewy bodies*. Proc Natl Acad Sci U S A, 1998. 95(11): p. 6469–73.
5. Hayakawa, H., et al., *Structurally distinct alpha-synuclein fibrils induce robust parkinsonian pathology*. Mov Disord, 2020. 35(2): p. 256–267.
6. Dhavale, D.D., et al., *Structure of alpha-synuclein fibrils derived from human Lewy body dementia tissue*. Nat Commun, 2024. 15(1): p. 2750.
7. Moors, T.E., et al., *The subcellular arrangement of alpha-synuclein proteoforms in the Parkinson's disease brain as revealed by multicolor STED microscopy*. Acta Neuropathol, 2021. 142(3): p. 423–448.
8. Shahmoradian, S.H., et al., *Lewy pathology in Parkinson's disease consists of crowded organelles and lipid membranes*. Nat Neurosci, 2019. 22(7): p. 1099–1109.
9. Kahle, P.J., et al., *Subcellular localization of wild-type and Parkinson's disease-associated mutant alpha -synuclein in human and transgenic mouse brain*. J Neurosci, 2000. 20(17): p. 6365–73.
10. Iwai, A., et al., *The precursor protein of non-A beta component of Alzheimer's disease amyloid is a presynaptic protein of the central nervous system*. Neuron, 1995. 14(2): p. 467–75.
11. Burre, J., et al., *Properties of native brain alpha-synuclein*. Nature, 2013. 498(7453): p. E4–6; discussion E6–7.
12. Gao, V., et al., *Functional and Pathological Effects of alpha-Synuclein on Synaptic SNARE Complexes*. J Mol Biol, 2023. 435(1): p. 167714.
13. Burre, J., et al., *Alpha-synuclein promotes SNARE-complex assembly in vivo and in vitro*. Science, 2010. 329(5999): p. 1663–7.
14. Baba, M., et al., *Aggregation of alpha-synuclein in Lewy bodies of sporadic Parkinson's disease and dementia with Lewy bodies*. Am J Pathol, 1998. 152(4): p. 879–84.
15. Yu, J. and Y.L. Lyubchenko, *Early stages for Parkinson's development: alpha-synuclein misfolding and aggregation*. J Neuroimmune Pharmacol, 2009. 4(1): p. 10–6.
16. Schmid, A.W., et al., *Alpha-synuclein post-translational modifications as potential biomarkers for Parkinson disease and other synucleinopathies*. Mol Cell Proteomics, 2013. 12(12): p. 3543–58.
17. Zhang, J., X. Li, and J.D. Li, *The Roles of Post-translational Modifications on alpha-Synuclein in the Pathogenesis of Parkinson's Diseases*. Front Neurosci, 2019. 13: p. 381.
18. van der Gaag, B.L., et al., *Distinct tau and alpha-synuclein molecular signatures in Alzheimer's disease with and without Lewy bodies and Parkinson's disease with dementia*. Acta Neuropathol, 2024. 147(1): p. 14.
19. Oueslati, A., *Implication of Alpha-Synuclein Phosphorylation at S129 in Synucleinopathies: What Have We Learned in the Last Decade?* J Parkinsons Dis, 2016. 6(1): p. 39–51.
20. Ramalingam, N., et al., *Dynamic physiological alpha-synuclein S129 phosphorylation is driven by neuronal activity*. NPJ Parkinsons Dis, 2023. 9(1): p. 4.

21. Parra-Rivas, L.A., et al., *Serine-129 phosphorylation of alpha-synuclein is an activity-dependent trigger for physiologic protein-protein interactions and synaptic function*. Neuron, 2023. 111(24): p. 4006–4023 e10.
22. Killinger, B.A., et al., *Distribution of phosphorylated alpha-synuclein in non-diseased brain implicates olfactory bulb mitral cells in synucleinopathy pathogenesis*. NPJ Parkinsons Dis, 2023. 9(1): p. 43.
23. Moors, T.E., et al., *Multi-platform quantitation of alpha-synuclein human brain proteoforms suggests disease-specific biochemical profiles of synucleinopathies*. Acta Neuropathol Commun, 2022. 10(1): p. 82.
24. Pradas, E. and M. Martinez-Vicente, *The Consequences of GBA Deficiency in the Autophagy-Lysosome System in Parkinson's Disease Associated with GBA*. Cells, 2023. 12(1).
25. Marques, A.R., et al., *Glucosylated cholesterol in mammalian cells and tissues: formation and degradation by multiple cellular beta-glucosidases*. J Lipid Res, 2016. 57(3): p. 451–63.
26. Akiyama, H. and Y. Hirabayashi, *A novel function for glucocerebrosidase as a regulator of sterylglucoside metabolism*. Biochim Biophys Acta Gen Subj, 2017. 1861(10): p. 2507–2514.
27. Brady, R.O., J.N. Kanfer, and D. Shapiro, *Metabolism of Glucocerebrosides. Ii. Evidence of an Enzymatic Deficiency in Gaucher's Disease*. Biochem Biophys Res Commun, 1965. 18: p. 221–5.
28. Mistry, P.K., et al., *Gaucher disease: Progress and ongoing challenges*. Mol Genet Metab, 2017. 120(1–2): p. 8–21.
29. Gan-Or, Z., et al., *Differential effects of severe vs mild GBA mutations on Parkinson disease*. Neurology, 2015. 84(9): p. 880–7.
30. Sidransky, E. and G. Lopez, *The link between the GBA gene and parkinsonism*. Lancet Neurol, 2012. 11(11): p. 986–98.
31. Parlar, S.C., et al., *Classification of GBA1 Variants in Parkinson's Disease: The GBA1-PD Browser*. Mov Disord, 2023. 38(3): p. 489–495.
32. den Heijer, J.M., et al., *A Large-Scale Full GBA1 Gene Screening in Parkinson's Disease in the Netherlands*. Mov Disord, 2020. 35(9): p. 1667–1674.
33. Ren, J., et al., *Comparing the effects of GBA variants and onset age on clinical features and progression in Parkinson's disease*. CNS Neurosci Ther, 2024. 30(2): p. e14387.
34. Tonin, R., et al., *GBA genotype-Parkinson's phenotype correlation in a cohort of 252 Italian patients from the Tuscany region*. Clinical Parkinsonism & Related Disorders, 2025. 12.
35. Clark, L.N., et al., *Association of glucocerebrosidase mutations with dementia with lewy bodies*. Arch Neurol, 2009. 66(5): p. 578–83.
36. Neumann, J., et al., *Glucocerebrosidase mutations in clinical and pathologically proven Parkinson's disease*. Brain, 2009. 132(Pt 7): p. 1783–94.
37. Nishioka, K., et al., *Glucocerebrosidase mutations in diffuse Lewy body disease*. Parkinsonism Relat Disord, 2011. 17(1): p. 55–7.
38. Gundner, A.L., et al., *Path mediation analysis reveals GBA impacts Lewy body disease status by increasing alpha-synuclein levels*. Neurobiol Dis, 2019. 121: p. 205–213.
39. Murphy, K.E., et al., *Reduced glucocerebrosidase is associated with increased alpha-synuclein in sporadic Parkinson's disease*. Brain, 2014. 137(Pt 3): p. 834–48.
40. Goker-Alpan, O., et al., *Glucocerebrosidase mutations are an important risk factor for Lewy body disorders*. Neurology, 2006. 67(5): p. 908–10.
41. Farrer, M.J., et al., *Glucosidase-beta variations and Lewy body disorders*. Parkinsonism Relat Disord, 2009. 15(6): p. 414–6.
42. Parkkinen, L., et al., *Glucocerebrosidase mutations do not cause increased Lewy body pathology in Parkinson's disease*. Mol Genet Metab, 2011. 103(4): p. 410–2.
43. Kurzawa-Akanbi, M., et al., *Altered ceramide metabolism is a feature in the extracellular vesicle-mediated spread of alpha-synuclein in Lewy body disorders*. Acta Neuropathol, 2021. 142(6): p. 961–984.
44. Moors, T.E., et al., *Characterization of Brain Lysosomal Activities in GBA-Related and Sporadic Parkinson's Disease and Dementia with Lewy Bodies*. Molecular Neurobiology, 2019. 56(2): p. 1344–1355.
45. Gegg, M.E., et al., *Glucocerebrosidase deficiency in substantia nigra of parkinson disease brains*. Ann Neurol, 2012. 72(3): p. 455–63.
46. Chiasserini, D., et al., *Selective loss of glucocerebrosidase activity in sporadic Parkinson's disease and dementia with Lewy bodies*. Mol Neurodegener, 2015. 10: p. 15.
47. Moors, T.E., et al., *Altered TFEB subcellular localization in nigral neurons of subjects with incidental, sporadic and GBA-related Lewy body diseases*. Acta Neuropathol, 2024. 147(1): p. 67.
48. Mazzulli, J.R., et al., *Gaucher disease glucocerebrosidase and alpha-synuclein form a bidirectional pathogenic loop in synucleinopathies*. Cell, 2011. 146(1): p. 37–52.
49. Xu, Y.H., et al., *Accumulation and distribution of alpha-synuclein and ubiquitin in the CNS of Gaucher disease mouse models*. Mol Genet Metab, 2011. 102(4): p. 436–47.
50. Yun, S.P., et al., *alpha-Synuclein accumulation and GBA deficiency due to L444P GBA mutation contributes to MPTP-induced parkinsonism*. Mol Neurodegener, 2018. 13(1): p. 1.
51. Fredriksen, K., et al., *Pathological alpha-syn aggregation is mediated by glycosphingolipid chain length and the physiological state of alpha-syn in vivo*. Proc Natl Acad Sci U S A, 2021. 118(50).
52. Bae, E.J., et al., *Loss of glucocerebrosidase 1 activity causes lysosomal dysfunction and alpha-synuclein aggregation*. Exp Mol Med, 2015. 47(10): p. e188.
53. Henderson, M.J., et al., *The Race to Salvage Glucocerebrosidase: Understanding Small-Molecule Therapies for GBA1-Associated Parkinsonism*. Mov Disord, 2025.

54. Menozzi, E., M. Toffoli, and A.H.V. Schapira, *Targeting the GBA1 pathway to slow Parkinson disease: Insights into clinical aspects, pathogenic mechanisms and new therapeutic avenues*. Pharmacol Ther, 2023. 246: p. 108419.
55. Huitinga, I. *Ethical and legal declaration of the Netherlands Brain Bank*. 2009; Available from: https://www.brainbank.nl/media/uploads/file/Ethical%20declaration%202019.pdf.
56. *BrainNet Europe Consortium - Code of Conduct*. 2008; Available from: https://www.brainbank.nl/media/uploads/file/Code-of-conduct.pdf.
57. Thal, D.R., et al., *Phases of Aβ-deposition in the human brain and its relevance for the development of AD*. Neurology, 2002. 58(12): p. 1791–1800.
58. Tunold, J.A., et al., *Lysosomal polygenic risk is associated with the severity of neuropathology in Lewy body disease*. Brain, 2023. 146(10): p. 4077–4087.
59. Blauwendraat, C., et al., *NeuroChip, an updated version of the NeuroX genotyping platform to rapidly screen for variants associated with neurological diseases*. Neurobiol Aging, 2017. 57: p. 247 e9–247 e13.
60. den Heijer, J.M., et al., *False negatives in GBA1 sequencing due to polymerase dependent allelic imbalance*. Sci Rep, 2021. 11(1): p. 161.
61. Andrews, S. *FastQC: A Quality Control Tool for High Throughput Sequence Data*. Available online at: http://www.bioinformatics.babraham.ac.uk/projects/fastqc/ 2010.
62. Bolger, A.M., M. Lohse, and B. Usadel, *Trimmomatic: a flexible trimmer for Illumina sequence data*. Bioinformatics, 2014. 30(15): p. 2114–2120.
63. Joshi, N. and J. Fass. *Sickle: A sliding-window, adaptive, quality-based trimming tool for FastQ files (Version 1.33) [Software]*. Available at https://github.com/najoshi/sickle.
64. Li, H. and R. Durbin, *Fast and accurate short read alignment with Burrows-Wheeler transform*. Bioinformatics, 2009. 25(14): p. 1754–1760.
65. McKenna, A., et al., *The Genome Analysis Toolkit: A MapReduce framework for analyzing next-generation DNA sequencing data*. Genome Research, 2010. 20(9): p. 1297–1303.
66. Kircher, M., et al., *A general framework for estimating the relative pathogenicity of human genetic variants*. Nature Genetics, 2014. 46(3): p. 310–+.
67. Cooper, G.M., et al., *Distribution and intensity of constraint in mammalian genomic sequence*. Genome Research, 2005. 15(7): p. 901–913.
68. Liu, X.M., et al., *WGSA: an annotation pipeline for human genome sequencing studies*. Journal of Medical Genetics, 2016. 53(2): p. 111–112.
69. Karczewski, K.J., et al., *The mutational constraint spectrum quantified from variation in 141,456 humans (vol 581, pg 434*, 2020). Nature, 2021. 590(7846): p. E53–E53.
70. Francioli, L.C., et al., *Whole-genome sequence variation, population structure and demographic history of the Dutch population*. Nature Genetics, 2014. 46(8): p. 818–825.
71. Jian, X., E. Boerwinkle, and X. Liu, *In silico prediction of splice-altering single nucleotide variants in the human genome*. Nucleic Acids Res, 2014. 42(22): p. 13534–44.
72. Jaganathan, K., et al., *Predicting Splicing from Primary Sequence with Deep Learning*. Cell, 2019. 176(3): p. 535–+.
73. Danis, D., et al., *Interpretable prioritization of splice variants in diagnostic next-generation sequencing*. Am J Hum Genet, 2021. 108(11): p. 2205.
74. Tunold, J.A., et al., *APOE and MAPT Are Associated With Dementia in Neuropathologically Confirmed Parkinson's Disease*. Front Neurol, 2021. 12: p. 631145.
75. Das, S., et al., *Next-generation genotype imputation service and methods*. Nat Genet, 2016. 48(10): p. 1284–1287.
76. Loh, P.R., et al., *Reference-based phasing using the Haplotype Reference Consortium panel*. Nat Genet, 2016. 48(11): p. 1443–1448.
77. Kan, A., et al., *An improved method for the detection and enrichment of low-abundant membrane and lipid raft-residing proteins*. J Proteomics, 2013. 79: p. 299–304.
78. Stojkovska, I. and J.R. Mazzulli, *Detection of pathological alpha-synuclein aggregates in human iPSC-derived neurons and tissue*. STAR Protoc, 2021. 2(1): p. 100372.
79. Gehrlein, A., et al., *Targeting neuronal lysosomal dysfunction caused by β-glucocerebrosidase deficiency with an enzyme-based brain shuttle construct*. Nature Communications, 2023. 14(1).
80. Urban, D.J., et al., *Optimization and Validation of Two Miniaturized Glucocerebrosidase Enzyme Assays for High Throughput Screening*. Combinatorial Chemistry & High Throughput Screening, 2008. 11(10): p. 817–824.
81. Berger, Z., et al., *Tool Compounds Robustly Increase Turnover of an Artificial Substrate by Glucocerebrosidase in Human Brain Lysates*. Plos One, 2015. 10(3).
82. R Core Team, *R: A Language and Environment for Statistical Computing*, in https://www.R-project.org/. 2023, R Foundation for Statistical Computing: Vienna, Austria.
83. RStudio Team, *RStudio: Integrated Development for R. RStudio*, in http://www.rstudio.com/. 2020, RStudio, PBC: Boston, USA.
84. Villanueva, R.A.M. and Z.J. Chen, *ggplot2: Elegant Graphics for Data Analysis, 2nd edition.* Measurement-Interdisciplinary Research and Perspectives, 2019. 17(3): p. 160–167.
85. Youden, W.J., *Index for rating diagnostic tests*. Cancer, 1950. 3(1): p. 32–5.
86. Alafuzoff, I., et al., *Staging/typing of Lewy body related alpha-synuclein pathology: a study of the BrainNet Europe Consortium*. Acta Neuropathol, 2009. 117(6): p. 635–52.
87. Montine, T.J., et al., *National Institute on Aging-Alzheimer's Association guidelines for the neuropathologic assessment of Alzheimer's disease: a practical approach*. Acta Neuropathol, 2012. 123(1): p. 1–11.

88. Mirra, S.S., et al., *The Consortium to Establish a Registry for Alzheimer's Disease (CERAD). Part II. Standardization of the neuropathologic assessment of Alzheimer's disease*. Neurology, 1991. 41(4): p. 479–86.
89. Slingerland, S., et al., *Cholinergic innervation topography in GBA-associated de novo Parkinson's disease patients*. Brain, 2024. 147(3): p. 900–910.
90. Olszewska, D.A., et al., *Association Between Glucocerebrosidase Mutations and Parkinson's Disease in Ireland*. Front Neurol, 2020. 11: p. 527.
91. Liu, G., et al., *Specifically neuropathic Gaucher's mutations accelerate cognitive decline in Parkinson's*. Ann Neurol, 2016. 80(5): p. 674–685.
92. Milanowski, L.M., et al., *Screening of GBA Mutations in Nigerian Patients with Parkinson's Disease*. Mov Disord, 2021. 36(12): p. 2971–2973.
93. Lesage, S., et al., *Large-scale screening of the Gaucher's disease-related glucocerebrosidase gene in Europeans with Parkinson's disease*. Hum Mol Genet, 2011. 20(1): p. 202–10.
94. Weerkamp, N.J., et al., *Diagnostic accuracy of Parkinson's disease and atypical parkinsonism in nursing homes*. Parkinsonism Relat Disord, 2014. 20(11): p. 1157–60.
95. di Biase, L., P.M. Pecoraro, and V. Di Lazzaro, *Validating the Accuracy of Parkinson's Disease Clinical Diagnosis: A UK Brain Bank Case-Control Study*. Ann Neurol, 2025. 97(6): p. 1110–1121.
96. Adler, C.H., et al., *Low clinical diagnostic accuracy of early vs advanced Parkinson disease: clinicopathologic study*. Neurology, 2014. 83(5): p. 406–12.
97. Rajput, A.H., B. Rozdilsky, and A. Rajput, *Accuracy of clinical diagnosis in parkinsonism–a prospective study*. Can J Neurol Sci, 1991. 18(3): p. 275–8.
98. Geut, H., et al., *Neuropathological correlates of parkinsonian disorders in a large Dutch autopsy series*. Acta Neuropathol Commun, 2020. 8(1): p. 39.
99. Espay, A.J. and A.J. Lees, *Beyond Pathology: alpha-Synuclein Homeostasis and Three Principles to Guide Research*. Mov Disord Clin Pract, 2025.
100. Espay, A.J. and A.J. Lees, *Loss of monomeric alpha-synuclein (synucleinopenia) and the origin of Parkinson's disease*. Parkinsonism Relat Disord, 2024. 122: p. 106077.
101. Anderson, J.P., et al., *Phosphorylation of Ser-129 is the dominant pathological modification of alpha-synuclein in familial and sporadic Lewy body disease*. J Biol Chem, 2006. 281(40): p. 29739–52.
102. Fujiwara, H., et al., *alpha-Synuclein is phosphorylated in synucleinopathy lesions*. Nat Cell Biol, 2002. 4(2): p. 160–4.
103. Ghanem, S.S., et al., *alpha-Synuclein phosphorylation at serine 129 occurs after initial protein deposition and inhibits seeded fibril formation and toxicity*. Proc Natl Acad Sci U S A, 2022. 119(15): p. e2109617119.
104. Morella, M.L., et al., *C-terminus-dependent detection of lysosomal alpha-synuclein in nigral Parkinson's disease human brain neurons*. Mol Neurodegener, 2025. 20(1): p. 116.
105. Leyns, C.E.G., et al., *Glucocerebrosidase activity and lipid levels are related to protein pathologies in Parkinson's disease*. NPJ Parkinsons Dis, 2023. 9(1): p. 74.
106. Rocha, E.M., et al., *Progressive decline of glucocerebrosidase in aging and Parkinson's disease*. Ann Clin Transl Neurol, 2015. 2(4): p. 433–8.
107. Huebecker, M., et al., *Reduced sphingolipid hydrolase activities, substrate accumulation and ganglioside decline in Parkinson's disease*. Mol Neurodegener, 2019. 14(1): p. 40.
108. Kloueva, N.M., M.C. Rademaker, and I. Huitinga, *Design of a European code of conduct for brain banking*. Handb Clin Neurol, 2018. 150: p. 51–81.

Figures

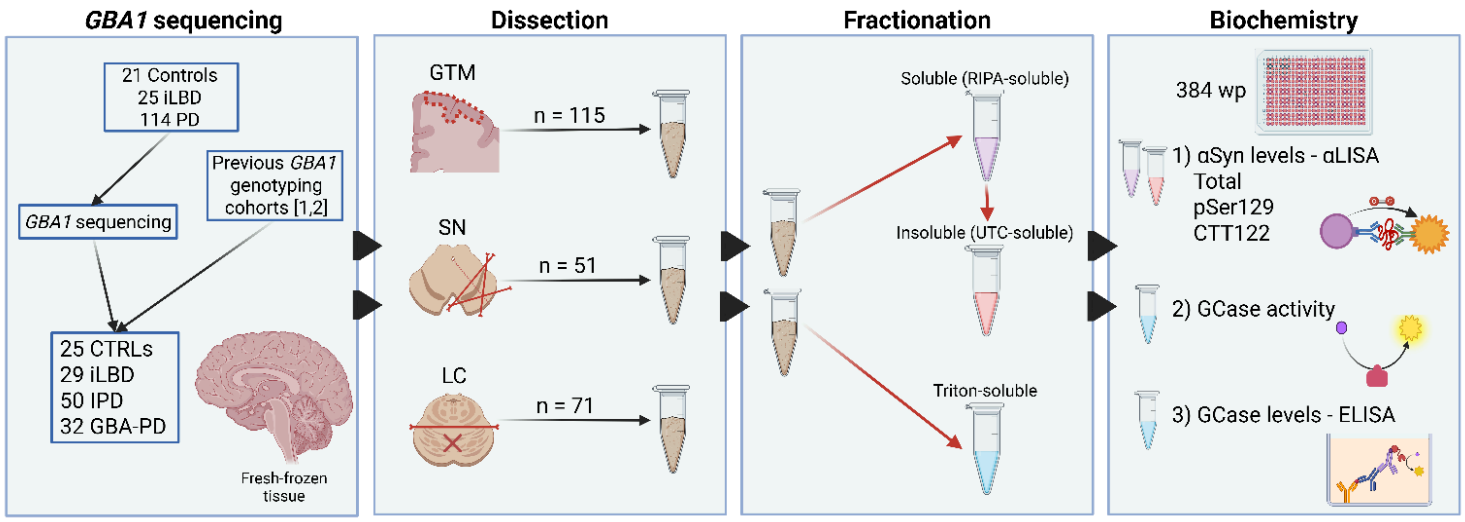

Figure 1

Workflow: selection, processing and biochemical analysis of frozen postmortem human brain tissue from a cohort of control, iLBD, idiopathic, and GBA-related PD subjects.

Graphical representation of the study design. The indicated incidental Lewy body disease (iLBD), Parkinson's disease (PD), and control cases were sequenced to identify cases with (GBA-PD) and without (IPD) *GBA1* risk variants. Together with additional cases from previous *GBA1* genotyping cohorts [44,

58], fresh-frozen tissue from the locus coeruleus (LC), substantia nigra (SN), and gyrus temporalis medius (GTM) was fractionated to extract Triton-soluble proteins (Triton-soluble fraction) and RIPA-soluble (Soluble fraction) proteins. Triton-insoluble UTC-soluble (Insoluble fraction) proteins were sequentially extracted from the RIPA-insoluble pellet. The Soluble and Insoluble fractions were used to measure Total (Total; detected with antibodies against aa 80-96 and aa 118-123), serine 129-phosphorylated (pSer129; detected with antibodies against aa 80-96 and pSer129), and C-terminal truncated at aa 122 (CTT122; detected with antibodies against aa 80-96 and CTT122) α-synuclein (αSyn) by AlphaLISA (1). Triton-soluble fractions were used to analyze Total glucocerebrosidase (GCase) enzyme activity assay and GCase protein levels by ELISA (2,3). aa = amino acid.

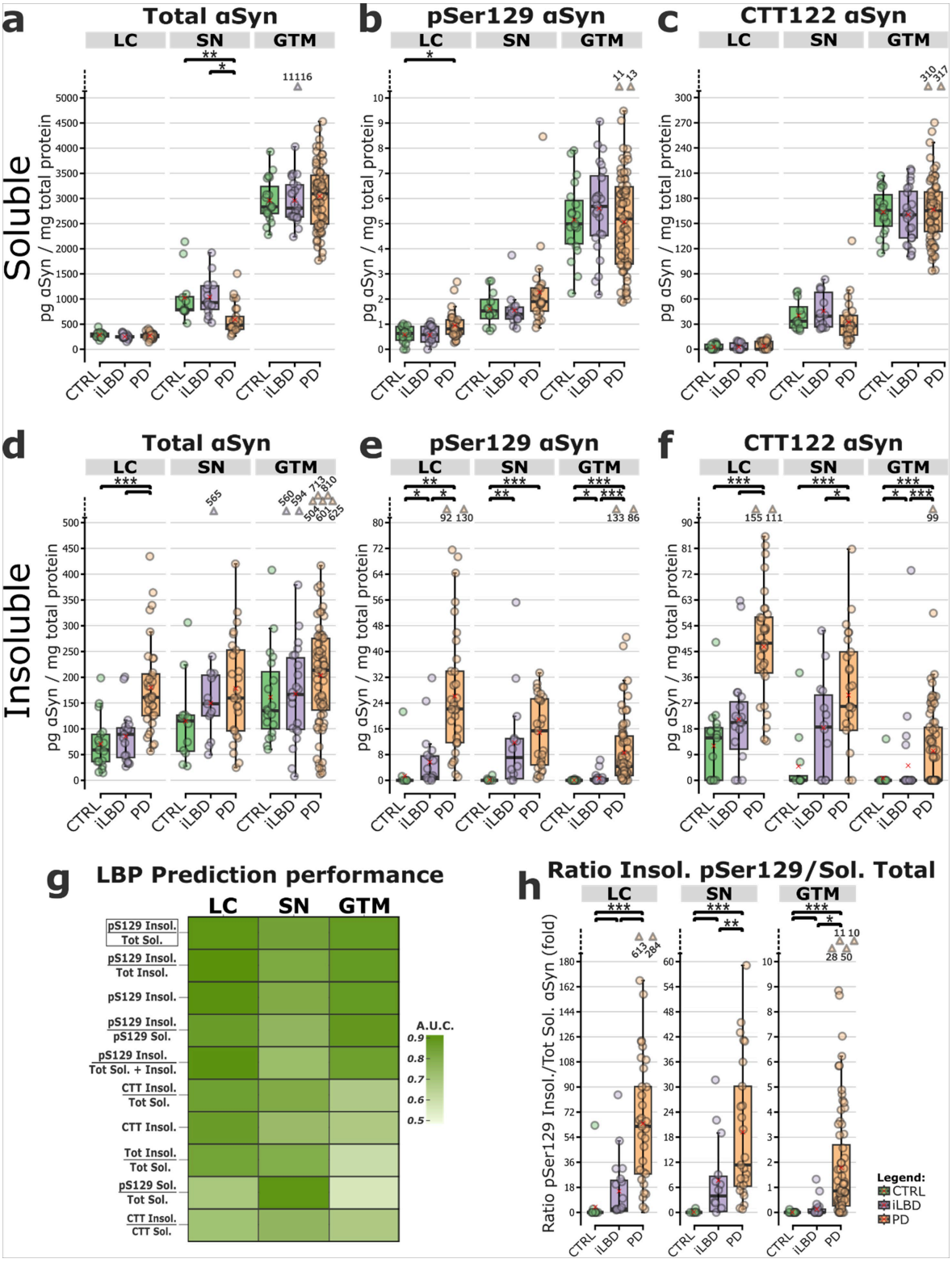

Figure 2

Insoluble pSer129 / Soluble Total α-synuclein ratio is increased in brain tissue of iLBD and PD compared to controls and predicts the presence of Lewy body pathology. a-f: Quantification of Total α-synuclein (αSyn; detected with antibodies against aa 80-96 and aa 118-123), serine 129-phosphorylated αSyn (pSer129; detected with antibodies against aa 80-96 and pSer129), and C-terminal truncated αSyn at aa 122 (CTT122; detected with antibodies against aa

80-96 and CTT122) by AlphaLISA in postmortem human brain tissue from individuals with incidental Lewy body disease (iLBD), Parkinson's disease (PD), and control (CTRL) cases. Fresh-frozen tissue from the substantia nigra (SN), locus coeruleus (LC), and gyrus temporalis medius (GTM) was sequentially extracted using RIPA buffer (Soluble) followed by UTC buffer (Insoluble). Results from the Soluble fraction (**a-c**) and Insoluble fraction (**d-f**) are normalized to total protein levels, showing an increase in α-synuclein protein levels in the Insoluble fraction across all regions, particularly in the pSer129 and CTT122 proteoforms. **g**: Area under the receiver operating characteristic curve (AUC) used to evaluate the performance of the readouts and their ratios in predicting the presence of Lewy body pathology (LBP) in each anatomical area. Readouts are ranked based on the sum of AUC in the three anatomical areas. **h**: Graph showing the best-performing predictor (Insoluble pSer129 αSyn / Soluble Total αSyn) expressed as fold change relative to the overall median. *p < 0.05; ** p < 0,01; ***p < 0.005; (generalized linear model + pairwise Tukey-adjusted estimated marginal means). aa = amino acid.

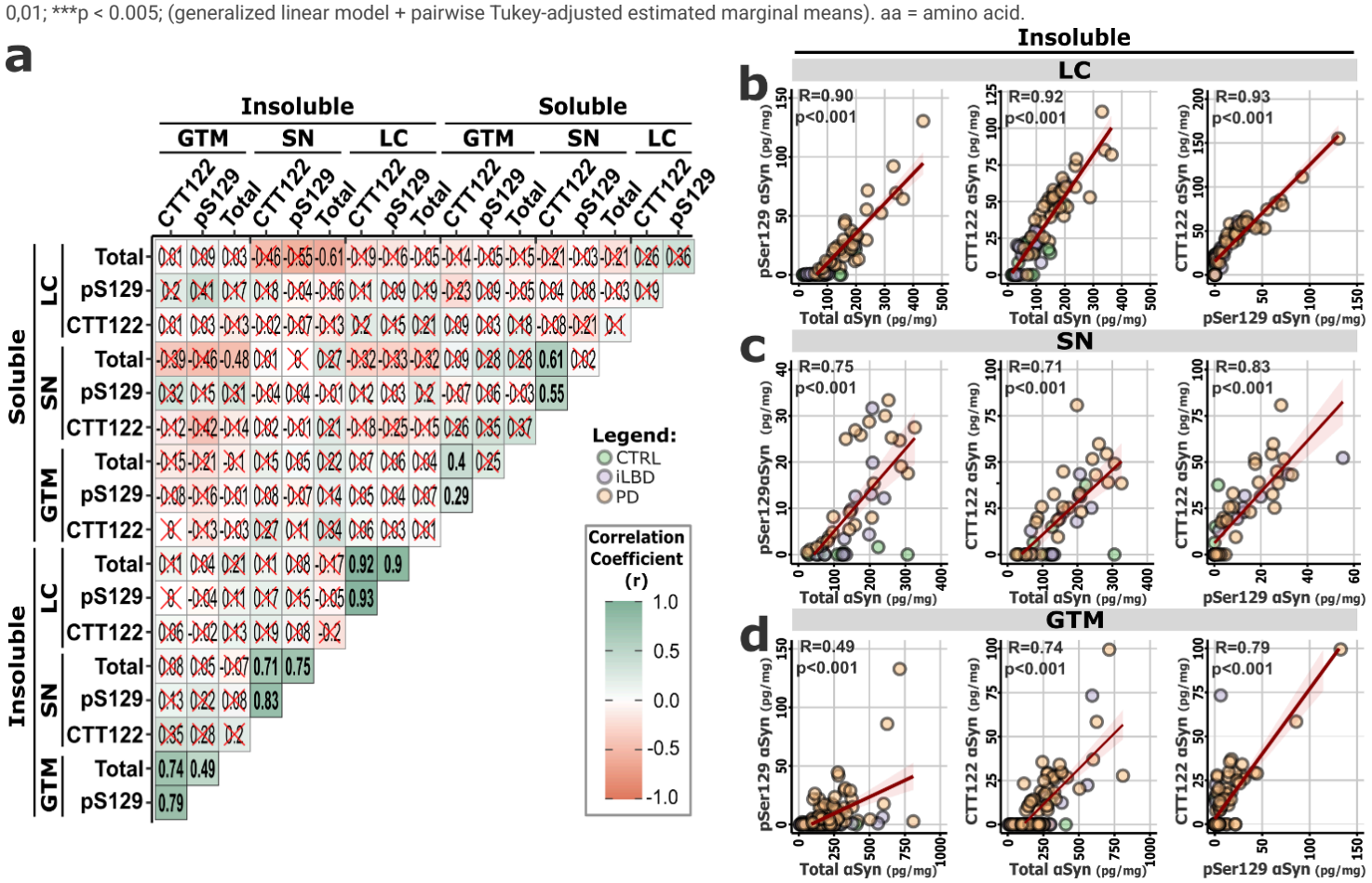

Figure 3

α-synuclein proteoforms correlate within the Insoluble fraction.

a: Multiple linear Pearson's correlation matrix between Total (aa 80-96-positive, aa 118-123-positive), serine 129-phosphorilated (pSer129; aa 80-96-positive, pSer129-positive), and aa 122 C-Term truncated (CTT122; aa 80-96-positive, CTT122-positive) α-synuclein (αSyn) levels in all anatomical areas showing no correlation within Soluble readouts, between Soluble and Insoluble readouts, and between measurements in different brain areas (n.s. correlations are crossed in red; p<0.05). The three αSyn proteoforms correlated within the Insoluble fraction. Non-significant results are crossed in red. **b-d**: Graphs of the correlation between the αSyn proteoforms in the Insoluble fraction in the LC (**b**), SN (**c**), and GTM (**d**). r = Pearson's correlation coefficient.

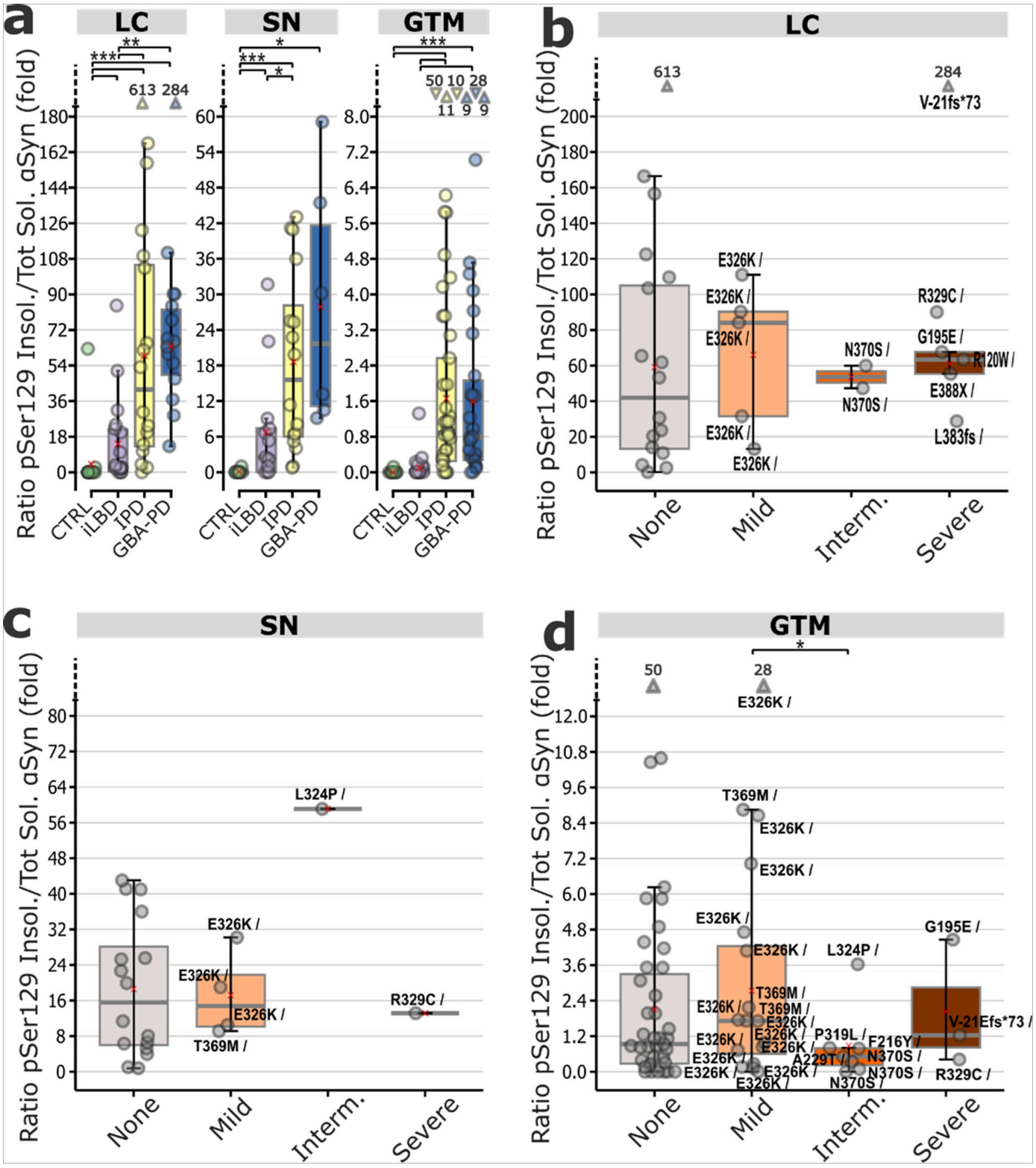

Figure 4

The Insoluble pSer129 / Soluble Total α-synuclein ratio is increased in GBA-related, idiopathic PD and iLBD cases compared to controls.
a: Comparison of Total αSyn (αSyn; detected with antibodies against aa 80-96 and aa 118-123), serine 129-phosphorylated αSyn (*p*Ser129; detected with antibodies against aa 80-96 and *p*Ser129), and C-terminal truncated αSyn at aa 122 (CTT122; detected with antibodies against aa 80-96 and CTT122) levels measured by AlphaLISA in postmortem brain tissue of controls (CTRL), incidental Lewy body disease (iLBD), and Parkinson's disease cases (PD) with (GBA-PD) and without (idiopathic; IPD) a *GBA1* risk variant. No difference is observed in the levels of Insoluble pSer129 αSyn in GBA-PD compared to IPD. **b-d:** αSyn levels across PD cases carrying different *GBA1* variants, classified based on variant severity (none, mild, intermediate, severe), in the three anatomical regions analyzed. αSyn levels are ratios of Insoluble pSer129 αSyn / Soluble Total αSyn expressed as fold change relative to the overall median. The quantification reveal minimal GBA-driven modulation of Insoluble pSer129 αSyn levels in PD. *p < 0.05; ** p < 0,01; ***p < 0.005; (generalized linear model + pairwise Tukey-adjusted estimated marginal means). aa = amino acid.

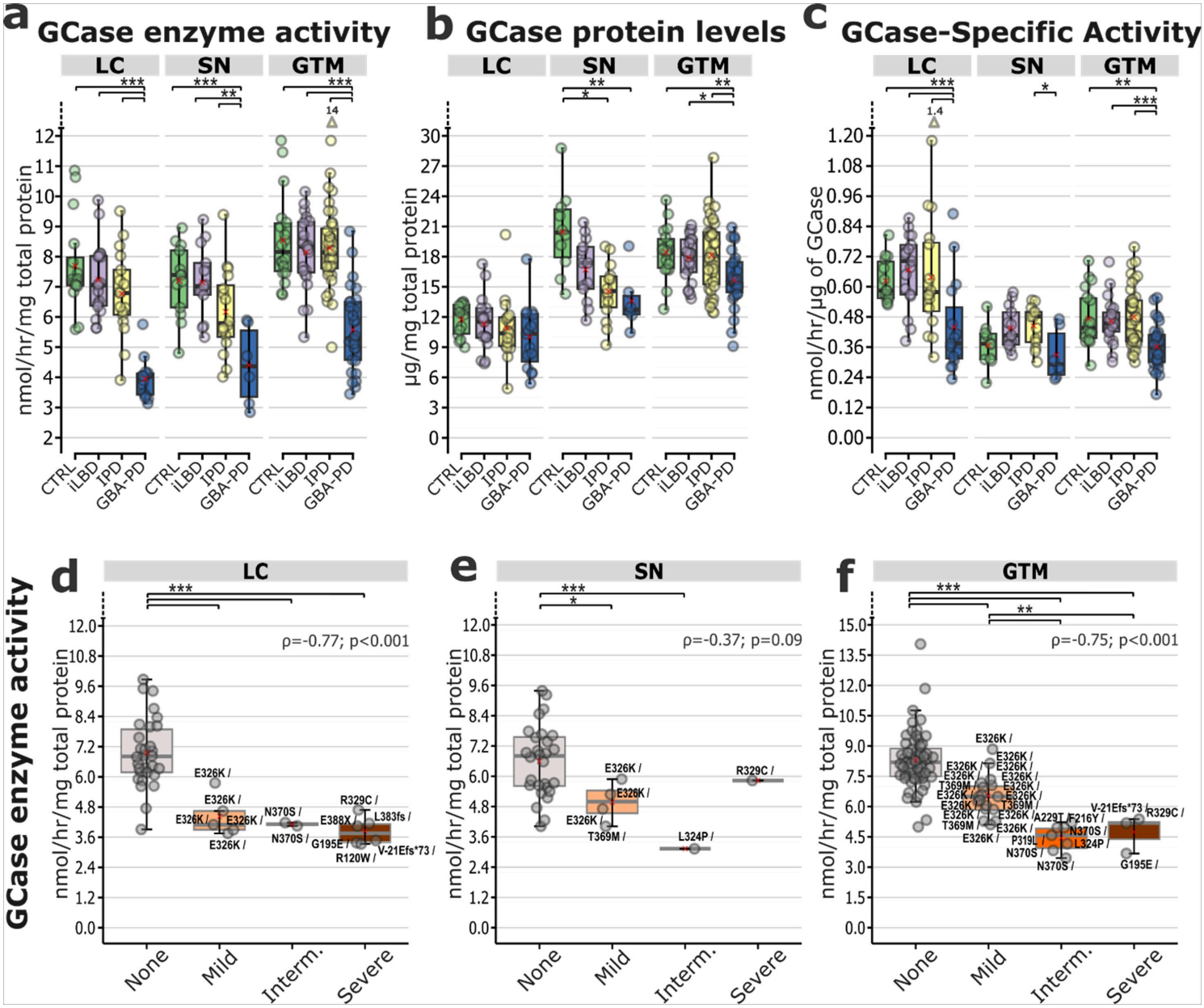

Figure 5

Total GCase activity is reduced in GBA-PD cases compared to idiopathic PD, iLBD, and controls.

a: Total glucocerebrosidase (GCase) enzyme activity normalized to total protein in control (CTRL), incidental Lewy body disease (iLBD), and Parkinson's disease (PD) cases, stratified by the presence (GBA-PD) or absence (idiopathic PD, IPD) of a *GBA1* risk variant. GCase activity is reduced in GBA-PD compared to the other groups **b**: GCase protein levels measured by ELISA and normalized to total protein. GCase level is reduced in GBA-PD compared to the other groups in SN and GTM. **c**: Total GCase enzyme activity normalized to GCase protein levels measured by ELISA is reduced in GBA-PD versus IPD. **d-f**: Comparison of total GCase enzyme activity among cases carrying different *GBA1* variants, classified based on variant severity (none, mild, intermediate, severe), across the three anatomical regions analyzed. Result indicate a negative correlation between *GBA1* nutation severity and measured GCase activity. *p < 0.05; ** p < 0,01; *** p < 0.005; (generalized linear model + pairwise Tukey-adjusted estimated marginal means). d-f: Spearman's correlation coefficient (ρ) and p value are reported per each panel.

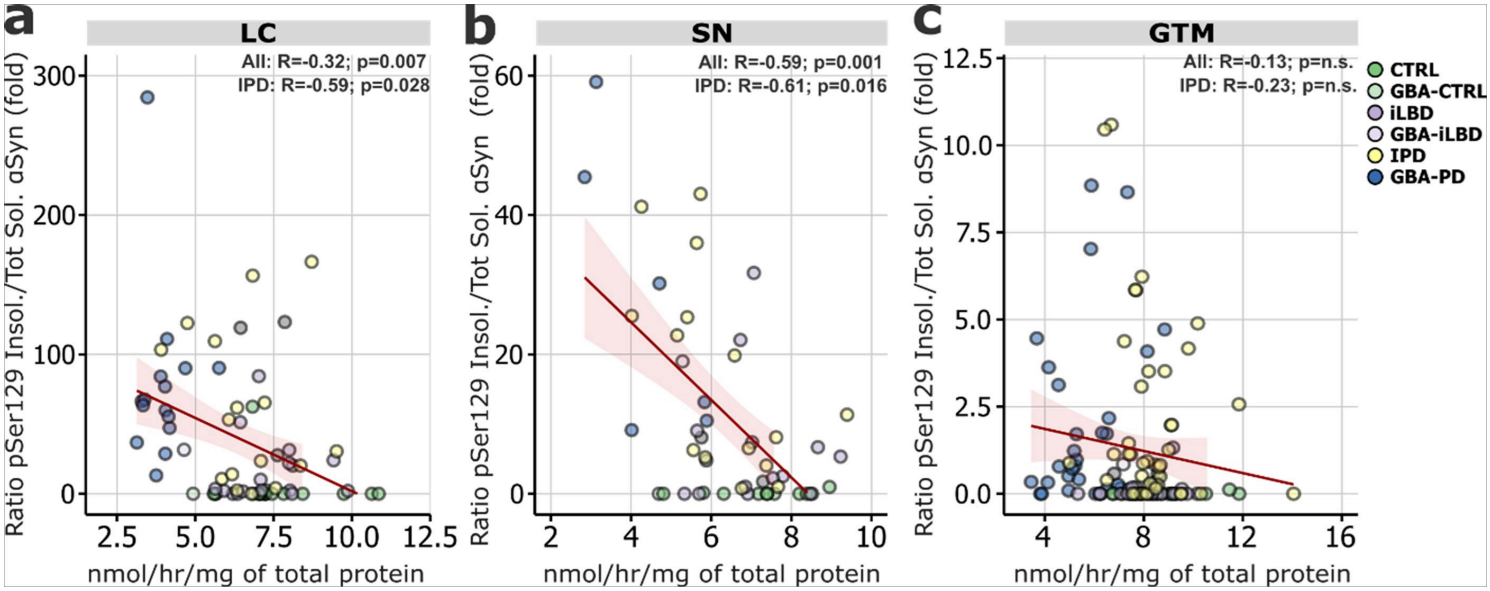

Figure 6

Insoluble pSer129 / Soluble Total α-synuclein ratio and total GCase activity correlate in post mortem human LBD brain.

a-c: Insoluble pSer129 / Soluble Total α-synuclein (αSyn) ratio and total glucocerebrosidase (GCase) activity negatively correlate in the *locus coeruleus* (LC; **a**), *substantia nigra* (SN; **b**), and *gyrus temporalis medius* (GTM; **c**). αSyn levels are ratios of Insoluble pSer129 αSyn / Soluble Total αSyn expressed as fold change relative to the overall median. Data are normalized to the median within each anatomical region. Pearson's correlation coefficient (R) and p values are reported within each panel.

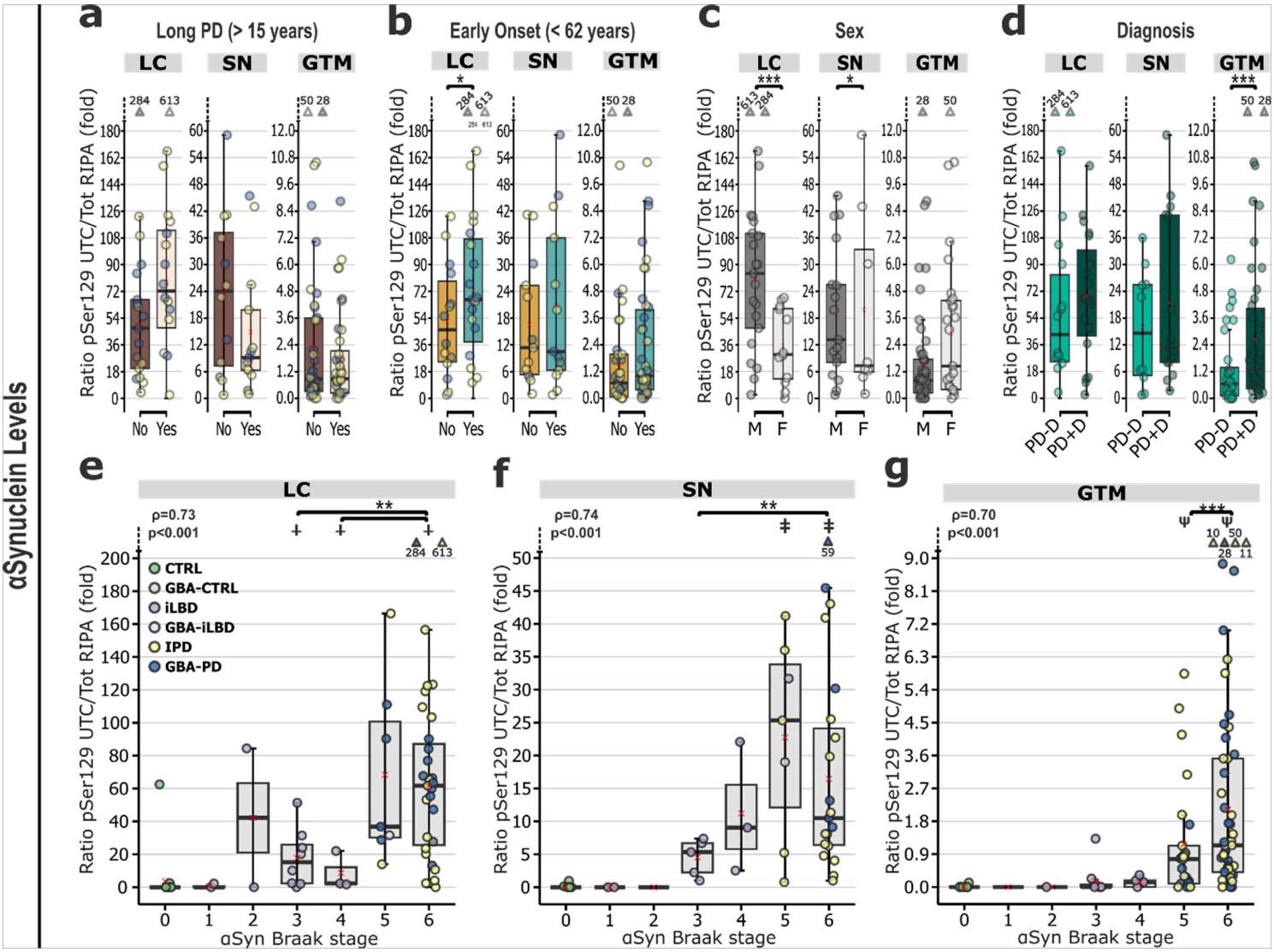

Figure 7

Ratio Insoluble pSer129 / Soluble Total α-synuclein correlates with Braak stage and dementia presence in the temporal cortex.

a-g: Analysis of the levels of Insoluble pSer129 / Soluble Total α-synuclein (αSyn) ratio between different clinical and neuropathological descriptors in the three brain areas. αSyn levels are expressed as fold change relative to the overall median **a**: Insoluble pSer129 / Soluble Total αSyn ratio levels in cases with short and long PD disease duration compared to median disease duration (15 years). **b**: Insoluble pSer129 / Soluble Total αSyn ratio levels in cases with early and late PD disease onset compared to median age at onset (62 years), showing an crease in Insoluble αSyn levels in cases with early disease onset in the LC. **c**: Insoluble pSer129 / Soluble Total αSyn ratio levels between female (F) and male (M) cases showing decreased Insoluble αSyn in females compared to males in LC and SN. **d**: Insoluble pSer129/ Soluble Total αSyn ratio levels between PD cases with (PD+D) and without (PD−D) dementia, showing an increase in Insoluble αSyn levels in the GTM in PDD cases. **e-g**: Insoluble pSer129 / Soluble Total αSyn ratio levels correlate with Braak αSyn stage in LC (**e**), SN (**f**) and GTM (**g**) showing high degree of correlation between the measures in all areas. *p < 0.05; ** p < 0,01; ***p < 0.005; ‡ p < 0.05 Vs. 0 and 1; ⍰ p < 0.05 Vs. 0,1 and 2; ψ p < 0.05 Vs. 0,1,2,3 and 4. a-d; h-k: ANCOVA analysis. e-g; l-n: multiple comparison with generalized linear model + pairwise Tukey-adjusted estimated marginal means. Correlation with Spearman's correlation. Spearman's rho correlation coefficient (ρ) and p value are presented in each panel.

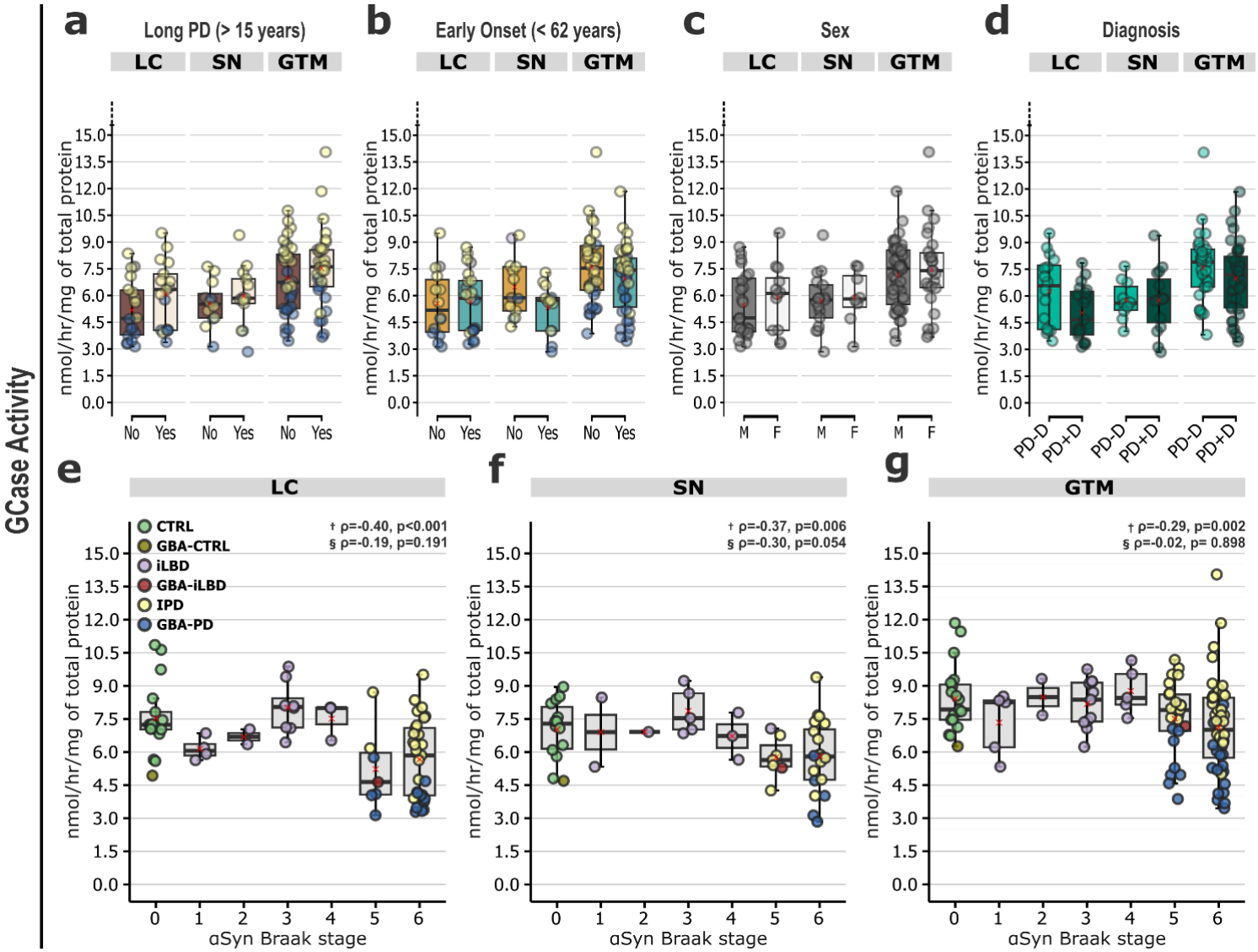

Figure 8

GCase activity correlates with Braak stage.

a-g: Total GCase activity levels between different clinical and neuropathological descriptors in the three brain areas. **a**: GCase activity levels in cases with short and long PD disease duration compared to median disease duration (15 years). **b**: GCase activity levels in cases with early and late PD disease onset compared to median age at onset (62 years) **c**: GCase activity levels between female (F) and male (M) subjects. **d**: Comparison of GCase activity levels between PD cases with (PD+D) and without (PD-D) dementia. **e-g**: Analysis of the correlation between Braak α-synuclein (αSyn) neuropathological scoring and total GCase activity levels in LC (**e**), SN (**f**) and GTM (**g**). Correlation with Spearman's correlation. Spearman's rho correlation coefficient (ρ) and p value are presented in each panel. §Spearman's correlation including GBA-PD cases. † Spearman's correlation excluding GBA-PD cases. ρ = correlation coefficient.